IEEE Access
Multidisciplinary ⋮ Rapid Review ⋮ Open Access Journal

Received 1 January 2025, accepted 8 January 2025, date of publication 13 January 2025, date of current version 17 January 2025.

Digital Object Identifier 10.1109/ACCESS.2025.3528772

RESEARCH ARTICLE

Disturbance Observer-Based Super-Twisting SMC for Variable Speed Wind Energy Conversion System Under Parametric Uncertainties

AHMAD BALA ALHASSAN[1], (Member, IEEE), MUHAMMAD AUWAL SHEHU[1], VIJAYAKUMAR GALI[2], (Senior Member, IEEE), AND TON DUC DO[1], (Senior Member, IEEE)

[1]Department of Robotics and Mechatronics, School of Engineering and Digital Sciences, Nazarbayev University, 010000 Astana, Kazakhstan
[2]Department of Electrical and Electronics Engineering, University of Hertfordshire, AL10 9AB Hatfield, U.K.

Corresponding author: Ton Duc Do (doduc.ton@nu.edu.kz)

This research was funded by the Science Committee of the Ministry of Science and Higher Education of the Republic of Kazakhstan with Grant no. AP22787355 and the Grant title 'Improving the Image Quality of Magnetic Particle Imaging by Optimizing the Scanning Paths'. This research was also funded by Nazarbayev University through the Social Policy Grant Program with Grant no. 201705 SPG.

ABSTRACT Effective control of the generator's shaft speed will ensure maximum power is captured from the wind turbines. However, the parameters of the wind energy conversion system (WECS)-based generators, including stator resistance and inductance, could change over time due to power loss, winding degradation, or core saturation. These parametric uncertainties affect the performance of the designed controllers. Although the sliding mode controllers (SMCs) are robust to matched uncertainties, the unmatched parametric uncertainties were not effectively compensated for by the SMC. This study investigated the performance of the SMC and super-twisting SMC (ST-SMC) under unmatched uncertainties using variable wind speed. Initially, the controllers were designed with the nominal parameters of the WECS-based permanent magnet synchronous generator (PMSG). Then, the values of the stator resistance and inductance were changed without changing the control design to test the robustness of the controllers to unmatched uncertainties. Finally, the uncertainties were estimated by the disturbance observer and incorporated into the controllers as a compensation mechanism. The controllers were designed using the synthetic wind profile and validated with the real-wind data. The transient and overall response of the controllers were analyzed using mean-absolute error (MAE) and root-mean-square error (RMSE) of the shaft speed tracking. The results demonstrated that the uncertainty compensation-based SMC/ST-SMC approach provides satisfactory shaft speed tracking performance even under parametric uncertainties.

INDEX TERMS Disturbance observer, wind speed estimation, sliding mode control (SMC), uncertainties, wind energy conversion system (WECS).

I. INTRODUCTION

Using fossil fuels for power generation has increased air pollution and led to global warming. This is obvious since about 25% of the world's population who reside in remote communities rely on fossil fuels to meet their energy needs. This emphasizes the need for cleaner alternate energy sources. One practical and most affordable solution for the increasing demand for clean energy is using renewable energy sources [1], [2]. As a sustainable alternative to conventional energy sources, renewable energy schemes such as hydro, solar, biomass, and wind, which are characterized by pollution-free features, are increasingly gaining popularity [3].

Due to its simple installation, ease of mobility, and environmental friendliness, wind energy, which is in abundance, is one of the fastest-growing and sought-after renewable energy sources. Wind energy can be harnessed by converting

The associate editor coordinating the review of this manuscript and approving it for publication was Ahmed F. Zobaa.

wind-induced mechanical energy from the rotating blade into electricity via generators. Based on the recent global wind report [4], in 2022 alone, the new wind farm installations, including offshore and onshore, have reached 77.6 GW. This is a notable increase of 53% from the 50.7 GW reported in 2018. Consequently, this notable surge underscores the growing need and widespread application of wind power generation scale globally. However, to optimally utilize the generated power, the existing standalone and isolated power wind farms need to be integrated with the grid. Remarkably, the grid-forming schemes have also been the focus of many researchers [5], [6], [7], [8]. Nonetheless, to have efficient integration of the wind farms, it is essential to have advanced control that is robust enough to eliminate the impact of frequency mismatch, harmonic distortions, and instability from the transient conditions, among others. Hence, Selvam et al. [9] presented a distribution static compensator (DSTATCOM) for the power distribution of WECS, which minimizes harmonic distortion and stabilizes the grid's varying parameters. Valladares et al. [10] investigated the possibilities of integrating the wind energy conversion system (WECS) with the grid using the hardware in the loop (HIL) configuration. The study demonstrated successful integration with effective DC link voltage stabilization.

Furthermore, the successful design, routine maintenance, and effective control of the energy conversion equipment are critical to the effective harnessing of electrical energy from the wind. Thus, to extract the maximum power from the wind, advanced control is necessary [11]. The WECS [12], [13], [14], [15], [16] is the most commonly used component for wind energy production. Thus, its control, which is the focus of this study, is crucial. In addition, it is worth noting that at each time interval when the wind profile varies, an optimal point exists where the turbine captures the maximum power. Interestingly, the rotor voltage of the generator can be regulated to extract this maximum power [17]. Conversely, the control of the WECS is difficult due to its parametric uncertainties and inherent nonlinearities. In this regard, a reliable and robust control scheme is essential for achieving the best performance of the WECS.

Remarkably, over the years, the study on WECS has garnered substantial consideration from scholars in numerous institutes and organizations around the world. Generally, doubly fed induction generators (DFIGs) and permanent magnet synchronous generators (PMSGs) are the most popular generators for the WECS application. The detailed performance analysis using different control approaches for the DFIG-based WECS was presented in [18]. For instance, using higher-order SMC, Mousavi et al. [19] employed an observer to compensate for the sensor faults associated with the DFIG. An adaptive fault-tolerant using SMC was presented for the DFIG-based WECS in [20]. Rauth et al. [21] proposed a sensorless control of DFIG-based WECS for start-up and grid integration.

Although DFIG is widely used for wind power generation, the PMSG, which is the focus of this study, has advantages over the DFIG. For instance, the PMSG can be used with full-scale converters, which allows for flexible, far-reaching control of the wind generator's power output. Its gearless configuration allows direct-drive operation, which reduces maintenance costs and improves efficiency. Another essential feature is that it operates at lower speeds, making it suitable for variable-speed wind turbines, and allows maximum power to be captured from varying wind profiles [22], [23]. However, in reality, the wind varies over a short period, and thus, the torque generated by the wind on the wind turbine's blade will change accordingly.

Recently, advancements in nonlinear control have emphasized the integration of disturbance observers (DOB) with SMC for enhanced robustness and tracking performance. For instance, Yang et al. [24] proposed an adaptive super-twisting SMC combined with an extended state observer for hydraulic systems, achieving asymptotic stability and chattering-free operation. Similarly, Yang et al. [25] introduced a DOB-based command-filtered control framework for uncertain nonlinear systems for handling mismatched disturbances while avoiding computational complexity. The torque generated by the wind can be estimated using DOBs, and subsequently, information on the corresponding reference speed of the generator is provided for optimal capture of the wind power.

In [26], a Takagi-Sugano fuzzy logic-based integral SMC was designed to estimate torque disturbance and control the WECS. Torchani et al. [27] presented a proportional-integral (PI) SMC by incorporating the effects of shaft stiffness into the PMSG dynamics using the mass-spring-damper concept. However, the study highlighted that the PI scheme affects the SMC's performance primarily due to nonlinearities. In [28], a robust finite time integral SMC for MPPT of the WECS in a standalone configuration. In related work, Zhang et al. [29] designed a super-twisting SMC technique combined with a time-varying two-time scale DOB, simplifying the traditional cascade control into a single-loop structure. Elsewhere, Zhang et al. [30] introduced a hybrid reaching law-based SMC with a time-varying nonlinear DOB, which effectively balances chattering reduction and fast convergence. The method demonstrated enhanced robustness against parameter uncertainties and external disturbances. Advancing this trend, Wang et al. [31] developed a model-free SMC strategy integrated with a finite-time generalized proportional integral observer, eliminating the dependency on motor parameters compared to conventional model-based methods.

As briefly highlighted above, the SMC has been a popular choice for the control WECS due to its applicability to linear and nonlinear systems, robustness to disturbances, and finite-time convergence, among others [32]. Nonetheless, the SMC is known for its chattering effect due to the discontinuous sign function, adversely affecting the actuators in practice. Interestingly, this phenomenon has been

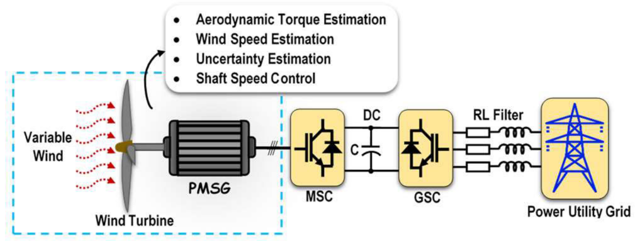

FIGURE 1. The conversion of wind into electrical energy using a (PMSG). The blue highlighted section is the focus of this study, which includes wind speed and aerodynamic torque estimation, parametric uncertainty estimation and compensation, and shaft speed control for optimal power harnessing.

extensively minimized by improving the design of the SMC through many approaches to WECS [33]. Nonetheless, the impact of unmatched parametric uncertainties still hinders the performance of the SMC.

The paper's content is divided into seven sections. The motivation and contribution of the work have been comprehensively highlighted in Section II. Section III briefly describes the maximum power point tracking (MPPT) and mathematical modeling of the PMSG-based WECS. Section IV presents the control design and the corresponding parametric uncertainty estimation techniques. Section V presents the stability assessment of the complete control system. Section VI presents the simulation results and analysis. Finally, Section VII discusses the conclusion of the whole study.

II. MOTIVATION AND CONTRIBUTION

As illustrated in Fig. I, the effective conversion of wind energy to electrical energy depends on the maximum power that can be harnessed from the wind at each instant. Multiple methods for maximum power point tracking (MPPT) exist, including extreme search [34], power signal feedback [35], and optimal gradient method [36], among others. Although these methods have been applied for the WECS, their complex computation, sensor delay, and cost limit their applications [34]. Another method is the use of tip-speed-ratio to achieve the MPPT, which depends on the torque generated by the wind energy on the turbine blades. However, calculating the torque is challenging, considering the varying nature of the wind. Therefore, the concept of disturbance observer is employed to estimate the aerodynamic torque in real-time using the generator's shaft speed information. In this regard, the shaft speed control is crucial and requires advanced controllers. However, since the WECS is highly nonlinear and prone to the influence of uncertainties, the control must be robust enough to reject the associated disturbances and uncertainties.

As highlighted in the introduction section, the SMC is a popular control for the WECS. One notable feature of the SMC is its robustness to matched disturbance. However, the unmatched disturbances that affect the system dynamics are not directly related to the control signal and, thus, were not satisfactorily rejected by the SMC. For machines (motors/generators), the stator inductance and resistance change over time due to various factors such as properties of the materials, operation conditions, and environmental factors. Typically, heat is dissipated when the machine operates over a long period due to power losses in the winding. The heat increases the temperature of the stator winding and, in turn, increases the resistance. In other cases, the insulation could degrade due to corrosion or mechanical stress, leading to high stator resistance. On the other hand, the degradation of the windings or the saturation of the magnetic core leads to a reduction of inductance.

In this study, the unmatched disturbances associated with parameters of the PMSG-based WECS were estimated using a disturbance observer for better compensation by the SMC. In addition, the aerodynamic torque is estimated using the higher-order exponential disturbance observer and incorporated into the MPPT algorithm. Moreover, a super-twisting SMC is designed to assess its robustness to uncertainties compared to the traditional SMC. Different wind profiles were used for a comprehensive analysis of the control schemes. The summary of the contribution of the paper can be summarized as follows:

1) Unlike the study by Chakri et al. [37], which uses an anemometer to measure the wind speed, this study uses aerodynamic torque observers, which provide sensorless estimation of the wind profile without the need for wind speed sensors (e.g., anemometer). This approach removes the cost of wind speed sensors and reduces the need for maintenance. It also provides faster and more accurate wind speed estimation in real-time for better MPPT and efficient shaft speed control.
2) In [38], [39], and [40], the authors estimated the uncertainties associated with WECS using a high-order observer (HODO) and compensated by a linear quadratic regulator (LQR). In this study, uncertainty estimation using an exponential DOB offers better estimation, and the shaft speed tracking performance was assessed using three different scenarios. The designed ST-SMC was investigated without uncertainties (nominal), with uncertainties (without compensation), and with uncertainties (with compensation). These cases allow the compensation mechanism and the robustness of the designed control scheme to be comprehensively analyzed under parametric uncertainties.
3) Previous studies generally used a single wind profile or even a fixed wind speed for the control design and analysis. This study used a synthetic wind profile for the control design and validated it with real-wind data. The results demonstrated that the ST-SMC approach can be successfully applied for shaft speed tracking even under the influence of parametric uncertainties and varying wind profiles.

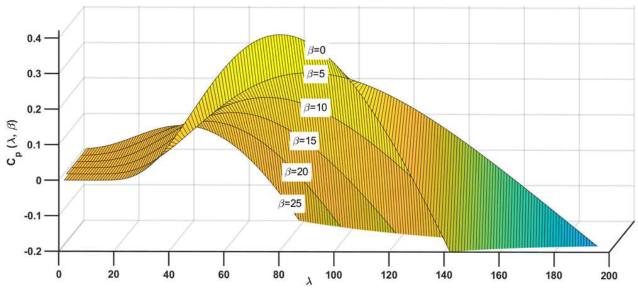

FIGURE 2. The relationship between power coefficient, C_p, and tip-speed-ratio, λ for different turbine pitch angle, β.

III. MAXIMUM POWER POINT TRACKING (MPPT) AND MODELING OF WIND TURBINE

This section presents the summarized dynamic model of the PMSG-based WECS presented in [41], [42], [43], [44], and [45].

A. MODELLING OF WIND TURBINE (WT) AND PMSG

Generally, the wind that acts on the wind turbine generates an aerodynamic power (P_w) as expressed in the following formulation [41]:

$$P_w(t) = \frac{1}{2}\rho\pi R_T^2 C_p(\lambda, \beta)v^3 \tag{1}$$

where v denotes the wind speed, $C_p(\lambda, \beta)$ denotes the power coefficient of the WT, which describes the amount of wind power to be harnessed on the turbine blade's pitch angle (β) and the tip-speed ratio (λ). R_T denotes the radius of the turbine, and ρ denotes the density of air (wind).

Although P_w represents a proportional relationship, the $C_p(\lambda, \beta)$ is generally experimentally determined based on the λ and β of the WT and is generally provided by the WT's manufacturer. It was investigated that for different β, there exists optimal, λ where the $C_p(\lambda, \beta)$ is maximum. This can be illustrated in Fig. 2 using the following formulation [42]:

$$\begin{cases} C_p(\lambda, \beta) = 0.5\left(\frac{116}{K_C} - 0.4\beta - 5\right)e^{-\left(\frac{21}{K_C}\right)}; \\ \frac{1}{K_C} = \left(\frac{1}{\lambda + 0.088\beta}\right) - \left(\frac{0.035}{\beta^3 + 1}\right) \end{cases} \tag{2}$$

Furthermore, the angular speed of the turbine (ω_T) is related to λ and v in the following relation [42]:

$$\lambda = \frac{\omega_T}{v}R_T \tag{3}$$

Then, the optimal reference turbine's shaft speed (ω_{ref}) can be derived from (3) as [38]:

$$\omega_{ref} = \frac{\lambda_{opt}}{R_T}v \tag{4}$$

where λ_{opt} is the optimal tip-slip-ratio at the point where the coefficient $C_p(\lambda, \beta)$ is maximum (see Fig. 2). On the other hand, the aerodynamic torque (T_a) that causes the turbine to rotate is related to the speed, ω_T, and the power, P_w, as [43]:

$$T_a(t) = \frac{P_w(t)}{\omega_T(t)} = \frac{1}{2}\rho\pi R_T^3 C_q(\lambda, \beta)v^2 \tag{5}$$

TABLE 1. Parameters of PMSG-based WECS.

S/N	Symbol	Parameter	Value
1	C_V	Coefficient of viscosity	0.002 kg.m²/s
2	E_J	Equivalent inertia of the rotor	7.856 kg.m²
3	S_R	Stator inductance	3.55 mH
4	S_L	Stator resistance	0.3676 Ω
5	N_P	Number of pole pairs	14
6	M_ψ	Magnitude flux linkage	0.2867 V.s/rad
7	R_T	Radius of rotor	1.84 m
8	λ_{opt}	Optimal tip-speed ratio	8.1
9	C_{p_max}	Maximum power coefficient	0.3262
10	ρ	Air density	1.25 kg/m³

Then, where the torque coefficient $C_q = C_p(\lambda, \beta)/\lambda$. In addition, the PMSGs are proven to have high efficiency and stability compared to other types of generators, as re-affirmed by the comparative analysis conducted in [44]. Thus, the PMSG-based WECS of (6) presented in [45] is adopted in this study, where $K_T = 3M_\psi P/2$. The parameters of the system are tabulated in Table 1.

$$\begin{cases} \frac{d\omega(t)}{dt} = -\frac{C_V}{E_J}\omega(t) - \frac{1}{E_J}T_e(t) + \frac{1}{E_J}T_a(t) \\ \frac{dT_e(t)}{dt} = -\frac{S_R}{S_L}T_e(t) - N_P K_T \omega(t) i_d(t) \\ -\frac{M_\psi N_P K_T}{S_L}\omega(t) + \frac{K_T}{S_L}V_q(t) \\ \frac{di_d(t)}{dt} = -\frac{S_R}{S_L}i_d(t) + \frac{N_P}{K_T}\omega(t)T_e(t) + \frac{1}{S_L}V_d(t) \end{cases} \tag{6}$$

B. PROBLEM DESCRIPTION

The main objective of this study is to control the angular speed of the generator effectively so that the wind turbine can harness the maximum wind energy. However, since the WECS is highly nonlinear and prone to the influence of uncertainties, the control must be robust enough to reject the associated disturbances and uncertainties. Therefore, considering the problem formulation of (6), the following assumptions were made before designing the controllers:

i. The shaft speed, ω(t), d-axis current, i_d(t), and electromagnetic, T_e(t) are the state variables i.e., they are accessible and could be measured with sensors.
ii. The aerodynamic parameters, v(t) and T_a(t), cannot be easily and accurately measured in real-time. Thus, they will be considered unavailable, and the dynamic disturbance observers will be designed to estimate them.
iii. The unmatched parametric uncertainties cannot be directly measured. Hence, the total uncertainties are considered a lumped disturbance to be estimated by the dynamic DOBs.

It is worth noting that a separate observer will be designed for the torque, T_a(t), and the uncertainties affecting V_q(t) and V_d(t) control signals, respectively. In each case, the higher-order estimators would be considered due to their improved estimation accuracy compared to the zero-order estimators.

IV. CONTROL DESIGN AND UNCERTAINTY ESTIMATION

In this section, the continuous super-twisting SMC (ST-SMC) was designed and compared with the traditional discontinuous SMC for shaft speed tracking and the current regulation. Three cases of the control structure would be investigated based on the ability of the control to reject or compensate for the uncertainties associated with the WECS.

A. DESIGN OF SUPER-TWISTING SMC (ST-SMC)

In SMC design, the sliding surface, which depends on the tracking path or regulation, is pre-defined. Herein, the ω(t) tracking error (ε_i) and the i_d(t) regulator (ε_c) are defined as:

$$\begin{cases} \varepsilon_\omega(t) = \omega_{ref}(t) - \omega(t) \\ \varepsilon_i(t) = i_d(t) - i_{ref}(t) \end{cases} \tag{7}$$

However, since the current is required to be regulated at zero for a surface-mounted PMSG, the $i_{\mathrm{ref}}(\mathrm{t}) = 0$. Then, the sliding surfaces for both the ω(t) and i_{d}(t) are defined as $Z_\omega(t)$ and $Z_i(t)$, respectively, to ensure asymptotic convergence of the speed tracking and current regulation as:

$$\begin{cases} Z_\omega(t) = \eta_s \varepsilon_\omega(t) + \dot{\varepsilon}_\omega(t) \\ Z_i(t) = \eta_i \left(i_d(t) - i_{ref}\right);\, i_{ref} = 0 \end{cases} \tag{8}$$

where η_{s} and η_{i} are the convergence gains, which define the tracking and regulation convergence speed, respectively. Also, since the sliding surface is expected to converge as time, t $\rightarrow$ ∞, the speed error dynamics of (8) can be represented as:

$$\dot{\varepsilon}_\omega(t) + \eta_s \varepsilon_\omega(t) = 0 \tag{9}$$

Theorem 1. Equation (9) is a first-order homogeneous differential equation with a solution of (10). Thus, it is obvious that depending on the magnitude η_s, the sliding surface Z_ω(t) will approach zero exponentially. Furthermore, a maximum convergence error exists at the initial tracking process i.e., t = t(0), which exponentially decays to zero:

$$\dot{\varepsilon}_\omega(t) = \varepsilon_\omega(t_0)e^{-\eta_s t} \;\Rightarrow\; |\varepsilon_\omega|_{\max} = |\varepsilon_\omega(t_0)| \tag{10}$$

Also, as the main objective of this study is to assess the effectiveness of the controller under parametric uncertainties, three cases of the control action were investigated as follows:

i) Case 1: Without uncertainties

In this scenario, the control design will be analyzed using the plant's nominal values, which will allow the exact behavior of the control system to be studied without any uncertainty. Thus, this case will demonstrate the best performance of the control and will serve as the benchmark for the analysis. Thus, the derivative of the sliding surfaces of (8) can be expressed as:

$$\begin{cases} \dot{Z}_\omega(t) = \eta_s \dot{\varepsilon}_\omega(t) + \ddot{\varepsilon}_\omega(t) \\ \quad = \ddot{\omega}_{ref}(t) + \eta_s \dot{\omega}_{ref}(t) - \Psi_A \omega(t) - \Psi_B \dot{T}_a(t) \\ -\Psi_C T_e(t) - \Psi_D \omega(t) i_d(t) + \Psi_E T_a(t) + \Psi_F V_q(t); \\ \dot{Z}_i(t) = \eta_i \left(-\dfrac{S_R}{E_L} i_d(t) + \dfrac{N_P}{K_T}\omega(t) T_e(t) + \dfrac{1}{E_L} V_d(t)\right) \end{cases} \tag{11}$$

where the constant parameters Ψ_{A}, Ψ_{B}, Ψ_{C}, Ψ_{D}, Ψ_{E}, and Ψ_{F} are defined for convenience of the formulation as follows as:

$$\begin{cases} \Psi_A = \left(\dfrac{C_V}{E_J}\left(\dfrac{C_v}{E_J} - \eta_s\right) + \dfrac{M_\psi N_P K_T}{E_J S_L}\right); \\ \Psi_B = \dfrac{1}{E_J}; \\ \Psi_C = \left(\dfrac{S_R}{S_L} + \dfrac{C_v}{E_J} - \eta_s\right)\dfrac{1}{E_J}; \\ \Psi_D = \dfrac{N_P K_T}{E_J}; \\ \Psi_E = \left(\dfrac{C_v}{E_J} - \eta_s\right)\dfrac{1}{E_J}; \\ \Psi_F = \dfrac{K_T}{E_J S_L} \end{cases} \tag{12}$$

Furthermore, the control signals V_q(t) and V_d(t) for the ω(t) and $\mathrm{i_d}$(t), respectively, can be expressed in (13), where $C_{SQ}(t)$ and $C_{SD}(t)$ are the switching control components of the controller to be designed. It is worth noting that the torque, T_a(t), the corresponding reference speed, ω_{ref}(t), and their derivatives cannot be measured directly. Thus, their estimates would be used by the controllers as illustrated as:

$$\begin{cases} V_{\mathrm{q}}(t) = \dfrac{1}{\Psi_{\mathrm{F}}}\begin{pmatrix} -\ddot{\hat{\omega}}_{\mathrm{ref}}(t) - \eta_s \dot{\hat{\omega}}_{\mathrm{ref}}(t) + \Psi_{\mathrm{A}}\omega(t) + \Psi_{\mathrm{B}}\dot{\hat{T}}_{\mathrm{a}}(t) \\ +\Psi_{\mathrm{C}} T_{\mathrm{e}}(t) + \Psi_{\mathrm{D}}\omega(t) i_{\mathrm{d}}(t) - \Psi_{\mathrm{E}}\hat{T}_{\mathrm{a}}(t) \end{pmatrix} \\ \quad + \dfrac{1}{\Psi_{\mathrm{F}}} C_{\mathrm{SQ}}(t); \\ V_{\mathrm{d}}(t) = \mathrm{S_R} i_{\mathrm{d}}(t) - \dfrac{\mathrm{E_L\, N_P}}{\mathrm{K_T}}\omega(t) T_{\mathrm{e}}(t) + \dfrac{\mathrm{E_L}}{\eta_i} C_{\mathrm{SD}}(t) \end{cases} \tag{13}$$

Finally, the two ST-SMCs for the ω(t) and $\mathrm{i_d}$(t) were designed based on (8), where μ_{Q1}, μ_{Q2}, μ_1, η_2, η_{D1}, and μ_{D2} are the positive control gains that determine the speed and convergence of the control action as follows:

$$\begin{cases} C_{\mathrm{SQ}}(t) = -\mu_{\mathrm{Q1}} |Z_\omega(t)|^{\delta_1} \operatorname{sign}(Z_\omega(t)) - \mu_{\mathrm{Q2}} \\ \qquad \displaystyle\int \operatorname{sign}(Z_\omega(t))\, \mathrm{d}t \\ C_{\mathrm{SD}}(t) = -\mu_{\mathrm{D1}} |Z_i(t)|^{\delta_2} \operatorname{sign}(Z_i(t)) - \mu_{\mathrm{D2}} \\ \qquad \displaystyle\int \operatorname{sign}(Z_i(t))\, \mathrm{d}t \\ \mu_{\mathrm{Q1}}, \mu_{\mathrm{Q2}}, \mu_{\mathrm{D1}}, \mu_{\mathrm{D2}} > 0 \quad ; \quad 0 < (\delta_1, \delta_2) < 1 \end{cases} \tag{14}$$

ii) Case 2: With uncertainties

In this scenario, the parameters of the PSMG-based WECS are changed. This reflects the reality of the system whereby the parameters can increase or change after continuous operation or due to changes in temperature and other environmental impacts. Thus, two constant parameters, stator resistance ($\mathrm{S_R}$) and stator inductance ($\mathrm{S_L}$) change or deviate from their respective nominal values. This phenomenon can be referred to as the uncertainty affecting the original system. Therefore, the original dynamics of (6) can be modified to include the resulting uncertainties $U_Q(t)$ and $U_D(t)$ affecting the control signals $V_q(t)$ and $V_d(t)$, respectively, as follows:

$$\begin{cases} \dfrac{d\omega(t)}{dt} = -\dfrac{C_V}{E_J}\omega(t) - \dfrac{1}{E_J}T_e(t) + \dfrac{1}{E_J}T_a(t) \\ \dfrac{dT_e(t)}{dt} = -\dfrac{S_R}{S_L}T_e(t) - N_P K_T \omega(t) i_d(t) - \dfrac{M_\psi N_P K_T}{S_L}\omega(t) \\ +\dfrac{K_T}{S_L}V_q(t) + U_Q(t) \\ \dfrac{di_d(t)}{dt} = -\dfrac{S_R}{S_L}i_d(t) + \dfrac{N_P}{K_T}\omega(t)T_e(t) + \dfrac{1}{S_L}V_d(t) + U_D(t) \end{cases} \tag{15}$$

These uncertainties, which relate to the changes in the system parameters, can be calculated for analysis using the formulation of (16). In reality, it would be difficult to quantify the exact variation of the individual parameter. As illustrated, if none of the parameters change, i.e., $\Delta\mathrm{S_R}$ and $\Delta\mathrm{S_L} = 0$, the uncertainties $U_Q(t)$ and $U_D(t)$ would certainly be zero. Thus, these parameters would be deliberately changed to analyze their behavior and impacts on the control system.

$$\begin{cases} U_Q(t) = \left(\dfrac{S_R}{S_L} - \left(\dfrac{S_R + \Delta S_R}{S_L + \Delta S_L}\right)\right)T_e(t) \\ +\left(\dfrac{M_\psi N_P K_T}{S_L} - \dfrac{M_\psi N_P K_T}{(S_L + \Delta S_L)}\right)\omega(t) \\ +\left(\dfrac{K_T}{S_L} - \dfrac{K_T}{(S_L + \Delta S_L)}\right)V_q(t) \\ U_D(t) = \left(\dfrac{S_R}{S_L} - \left(\dfrac{S_R + \Delta S_R}{S_L + \Delta S_L}\right)\right)i_d(t) \\ +\left(\dfrac{1}{S_L} - \dfrac{1}{(S_L + \Delta S_L)}\right)V_d(t) \end{cases} \tag{16}$$

Assumption 1: The WECS perturbation terms $\mathrm{U_Q(t)}$ and $\mathrm{U_D(t)}$ are considered as upper-bounded and satisfy the Lipschitz continuity condition such that $|\mathrm{U_Q(t)}| \leq \Omega_Q$ and $|\mathrm{U_D(t)}| \leq \Omega_D$, where $\Omega_Q \in \Re^+$ and $\Omega_D \in \Re^+$ are upper-limits.

iii) Case 3: Control with uncertainty compensation

In this case, the uncertainty terms of (16) were incorporated into the control signal of (13) using the procedure of (7) to (12). After simplification, the control signals can be expressed in (17). However, the uncertainty terms cannot be measured by the controller. Thus, the estimated uncertainties, which would be determined using a disturbance observer, would be utilized. In this analysis, the controller has prior knowledge of the uncertainties, and its compensating terms are incorporated into the control signal. Thus, the effectiveness of the control for disturbance rejection would be assessed.

$$\begin{cases} V_q(t) = \dfrac{1}{\Psi_F}\begin{pmatrix} -\ddot{\hat{\omega}}_{ref}(t) - \eta_s\dot{\hat{\omega}}_{ref}(t) + \Psi_A\omega(t) + \Psi_B\dot{\hat{T}}_a(t) \\ +\Psi_C T_e(t) + \Psi_D\omega(t)i_d(t) - \Psi_E\hat{T}_a(t) \end{pmatrix} \\ -\dfrac{S_L}{K_T}\hat{U}_Q(t) + \dfrac{1}{\Psi_F}C_{SQ}(t); \\ V_d(t) = S_R i_d(t) - \dfrac{S_L N_P}{K_T}\omega(t)T_e(t) - S_L\hat{U}_D(t) + \dfrac{S_L}{\eta_i}C_{SD}(t) \end{cases} \tag{17}$$

where $C_{SQ}(t)$ and $C_{SD}(t)$ are the switching control components of the controller expressed in (14), while $\hat{U}_Q(t)$ and $\hat{U}_D(t)$ are the DOB estimates of the perturbations $U_Q(t)$ and $U_D(t)$, respectively.

Assumption 2: To simplify the subsequent stability analysis, in addition to *assumption 1*, the perturbations are assumed to obey the following:

$$\frac{S_L}{K_T}U_Q(t) \leq \mho_Q\,|Z_\omega(t)|^{\delta_1} \tag{18}$$

$$S_L U_D(t) \leq \mho_D\,|Z_i(t)|^{\delta_2} \tag{19}$$

with the controller parameters δ_1 and δ_2 as in (14) while $\mho_Q \in \Re^+$ and $\mho_D \in \Re^+$ are upper-limits.

B. TORQUE AND UNCERTAINTY ESTIMATION

According to the control laws of (17), it is obvious that the uncertainties, $U_Q(t)$ and $U_D(t)$, the torque, $T_a(t)$, and its variants, including the ω_{ref}, were not directly available to the control. Thus, they need to be estimated using dynamic estimators. However, the $T_a(t)$ was estimated and analyzed in our previous study [46]; hence, it would be considered a known or measurable term. Nonetheless, the $U_Q(t)$ and $U_D(t)$ would be estimated using the higher-order exponential disturbance observer (HOEDO) as expressed in (20) and (21). The HOEDO was chosen because it can provide more accurate estimations than traditional observers.

$$\begin{cases} \hat{U}_Q(t) = \varnothing_1(t) + \mathbb{N}_1^q T_e(t) \\ \dot{\hat{U}}_Q(t) = \varnothing_2(t) + \mathbb{N}_2^q T_e(t) \\ \ddot{\hat{U}}_Q(t) = \varnothing_3(t) + \mathbb{N}_3^q T_e(t) \\ \dot{\varnothing}_1(t) = -\mathbb{N}_1^q\begin{pmatrix} -\frac{S_R}{S_L}T_e(t) - N_P K_T\omega(t)i_d(t) \\ -\frac{M_\psi N_P K_T}{S_L}\omega(t) + \frac{K_T}{S_L}V_q(t) + \hat{U}_Q(t) \end{pmatrix} + \dot{\hat{U}}_Q(t) \\ \dot{\varnothing}_2(t) = -\mathbb{N}_2^q\begin{pmatrix} -\frac{S_R}{S_L}T_e(t) - N_P K_T\omega(t)i_d(t) \\ -\frac{M_\psi N_P K_T}{S_L}\omega(t) + \frac{K_T}{S_L}V_q(t) + \hat{U}_Q(t) \end{pmatrix} + \ddot{\hat{U}}_Q(t) \\ \dot{\varnothing}_3(t) = -\mathbb{N}_3^q\begin{pmatrix} -\frac{S_R}{S_L}T_e(t) - N_P K_T\omega(t)i_d(t) \\ -\frac{M_\psi N_P K_T}{S_L}\omega(t) + \frac{K_T}{S_L}V_q(t) + \hat{U}_Q(t) \end{pmatrix} \end{cases} \tag{20}$$

$$\begin{cases} \hat{U}_D(t) = \Upsilon_1(t) + \mathbb{N}_1^d i_d(t) \\ \dot{\hat{U}}_D(t) = \Upsilon_2(t) + \mathbb{N}_2^d i_d(t) \\ \ddot{\hat{U}}_D(t) = \Upsilon_3(t) + \mathbb{N}_3^d i_d(t) \\ \dot{\Upsilon}_1(t) = -\mathbb{N}_1^d \begin{pmatrix} -\frac{S_R}{S_L} i_d(t) + \frac{N_P}{K_T}\omega(t)T_e(t) \\ +\frac{1}{S_L}V_d(t) + \hat{U}_D(t) \end{pmatrix} + \dot{\hat{U}}_D(t) \\ \dot{\Upsilon}_2(t) = -\mathbb{N}_2^d \begin{pmatrix} -\frac{S_R}{S_L} i_d(t) + \frac{N_P}{K_T}\omega(t)T_e(t) \\ +\frac{1}{S_L}V_d(t) + \hat{U}_D(t) \end{pmatrix} + \ddot{\hat{U}}_D(t) \\ \dot{\Upsilon}_3(t) = -\mathbb{N}_3^d \begin{pmatrix} -\frac{S_R}{S_L} i_d(t) + \frac{N_P}{K_T}\omega(t)T_e(t) \\ +\frac{1}{S_L}V_d(t) + \hat{U}_D(t) \end{pmatrix} \end{cases} \tag{21}$$

where $\emptyset_i(t)$ and $\Upsilon_i(t)$ denote the observer auxiliary variables, $\mathrm{N}_\mathrm{i}^\mathrm{q}$ and $\mathrm{N}_\mathrm{i}^\mathrm{d}$ represent the observer gains for the $U_Q(t)$ and $U_D(t)$ estimations, respectively, for $i = 1,2,3$.

Analysis of Estimation Convergence: The approach for the convergence analysis of $U_Q(t)$ and $U_D(t)$ would be similar. Thus, one observer is considered, whereby the estimation error is defined in (22). After substituting the estimation formulation and using the system dynamics of (6), the error dynamics can be expressed in (23).

$$\begin{cases} \tilde{U}_{Q1}(t) = U_Q(t) - \hat{U}_Q(t) \ ; \\ \tilde{U}_{Q2}(t) = \dot{U}_Q(t) - \dot{\hat{U}}_Q(t) \ ; \\ \tilde{U}_{Q3}(t) = \ddot{U}_Q(t) - \ddot{\hat{U}}_Q(t) \end{cases} \tag{22}$$

$$\begin{cases} \dot{\tilde{U}}_{Q1}(t) = \tilde{U}_{Q2}(t) - \mathbb{N}_1^q \tilde{U}_{Q1}(t) \\ \dot{\tilde{U}}_{Q2}(t) = \tilde{U}_{Q3}(t) - \mathbb{N}_2^q \tilde{U}_{Q1}(t) \\ \dot{\tilde{U}}_{Q3}(t) = -\mathbb{N}_3^q \tilde{U}_{Q1} \end{cases}$$

$$\Rightarrow \begin{bmatrix} \dot{\tilde{U}}_{Q1}(t) \\ \dot{\tilde{U}}_{Q2}(t) \\ \dot{\tilde{U}}_{Q3}(t) \end{bmatrix} = \begin{bmatrix} -\mathbb{N}_1^q & 1 & 0 \\ -\mathbb{N}_2^q & 0 & 1 \\ -\mathbb{N}_3^q & 0 & 0 \end{bmatrix} \begin{bmatrix} \tilde{U}_{Q1}(t) \\ \tilde{U}_{Q2}(t) \\ \tilde{U}_{Q3}(t) \end{bmatrix} \tag{23}$$

Theorem 2. According to the error formulation of (23), the corresponding characteristics equation can be determined in (24). Therefore, it is obvious that if the observer gains N_i^q *and* N_i^d for the $U_Q(t)$ and $U_D(t)$ are calculated such that (24) is Hurwitz [47], the uncertainty estimation errors will decay to zero asymptotically.

$$\begin{cases} s^3 + \mathbb{N}_1^q s^2 + \mathbb{N}_2^q s + \mathbb{N}_3^q = 0 \\ s^3 + \mathbb{N}_1^d s^2 + \mathbb{N}_2^d s + \mathbb{N}_3^d = 0 \end{cases} \tag{24}$$

Remark 1: Generally, low wind speeds are much easier to estimate due to the slow varying nature of the wind profile. The high wind speed is often challenging to estimate satisfactorily. In this regard, many researchers assumed wind profiles to vary slowly, simplifying the torque estimation. However, in reality, the wind speed can change fast, which requires better estimation techniques. In our recent preliminary study [46], the performance of the proposed estimation was investigated for a wide range of wind speeds ranging from low to extremely fast-changing profiles. In all cases, the observer can effectively estimate a wide range of wind profiles, including low and high speeds.

V. STABILITY ANALYSIS OF THE CONTROL SYSTEM

In this section, the stability of the closed-loop WECS is investigated, and formulations to estimate the finite-time convergences of trajectories will also be derived. We will analyze the stability of the closed-loop system for the case with uncertainties and DOB estimates.

In the event that *assumption 2* is satisfied, the super-twisting control design parameters $\mu_{\mathrm{Q1}} \in \Re^+$, $\mu_{\mathrm{Q2}} \in \Re^+$, $\mu_{\mathrm{D1}} \in \Re^+$, and $\mu_{\mathrm{D2}} \in \Re^+$can be designed based on the relationship [48]:

$$\begin{cases} \mu_{\mathrm{Q1}} > 2\mho_{\mathrm{Q}}; & \mu_{\mathrm{Q2}} \geq \mu_{\mathrm{Q1}} \dfrac{5\mu_{\mathrm{Q1}} + 4\mho_{\mathrm{Q}}}{2\left(\mu_{\mathrm{Q1}} - 2_{\mathrm{Q}}\right)} \mho_{\mathrm{Q}} \\ \mu_{\mathrm{D1}} > 2\mho_{\mathrm{D}}; & \mu_{\mathrm{D2}} \geq \mu_{\mathrm{D1}} \dfrac{5\mu_{\mathrm{D1}} + 4\mho_{\mathrm{D}}}{2\left(\mu_{\mathrm{D1}} - 2\mho_{\mathrm{D}}\right)} \mho_{\mathrm{D}} \end{cases} \tag{25}$$

Theorem 2: For the WECS of (15) in the context of (16) and estimators (20) and (21), if the sliding surfaces are designed as (8) and the control laws designed as (17) and (14) with gains satisfying (25), then the sliding surfaces $Z_\omega(t)$ and $Z_i(t)$ are bounded-time stable. Moreover, estimates of convergence times for trajectories originating at $Z_\omega(0) = Z_{\omega_0}$ and $Z_i(0) = Z_{i_0}$ are respectively not larger than:

$$\begin{cases} \mathrm{T}_{Z_\omega} = \dfrac{\lambda_{\max}\left\{\mathrm{P}_{Z_\omega}\right\}}{\delta_1 \lambda_{\min}^{\delta_1}\left\{\mathrm{P}_{Z_\omega}\right\}\lambda_{\min}\left\{\mathrm{Q}_{Z_\omega}\right\}} V_\omega^{\delta_1}\left\{Z_{\omega 0}\right\} \\ \mathrm{T}_{Z_i} = \dfrac{\lambda_{\max}\left\{\mathrm{P}_{Z_i}\right\}}{\delta_2 \lambda^{\delta_2}{}_{\min}\left\{\mathrm{P}_{Z_i}\right\}\lambda_{\min}\left\{\mathrm{Q}_{Z_i}\right\}} V_i^{\delta_2}\left\{Z_{i0}\right\} \end{cases} \tag{26}$$

Proof of Theorem 2: Like in the recent work of Alhassan et al. [49], let us take two positive definite (PD) functions V_ω and V_i which are radially unbounded (RU) in Euclidean space as possible Lyapunov functions given by:

$$\begin{cases} V_\omega = \xi_\omega^{\mathrm{T}} \mathrm{P}_{Z_\omega} \xi_\omega \\ V_i = \xi_i^{\mathrm{T}} \mathrm{P}_{Z_i} \xi_i \end{cases} \tag{27}$$

where $\xi_\omega \in \Re^{2\times 1}$, $\xi_i \in \Re^{2\times 1}$, $\mathrm{P}_{Z_\omega} \in \Re^{2\times 2}$, and $\mathrm{P}_{Z_i} \in \Re^{2\times 2}$, are, respectively, defined as follows:

$$\begin{cases} \xi_\omega = \begin{bmatrix} \xi_{\omega 1} & \xi_{\omega 2} \end{bmatrix}^{\mathrm{T}} = \begin{bmatrix} |Z_\omega(t)|^{\delta_1} \operatorname{sign}(Z_\omega(t)) & W_\omega \end{bmatrix}^{\mathrm{T}} \\ \xi_i = \begin{bmatrix} \xi_{i1} & \xi_{i2} \end{bmatrix}^{\mathrm{T}} = \begin{bmatrix} |Z_i(t)|^{\delta_2} \operatorname{sign}(Z_i(t)) & W_i \end{bmatrix}^{\mathrm{T}} \end{cases} \tag{28}$$

$$W_\omega = \mu_{\mathrm{Q2}} \int \operatorname{sign}(Z_\omega(t))\,\mathrm{d}t; \; W_i = \mu_{\mathrm{D2}} \int \operatorname{sign}(Z_i(t))\,\mathrm{d}t$$

$$\begin{cases} \mathrm{P}_{Z_\omega} = \dfrac{1}{2}\begin{bmatrix} \mu_{\mathrm{Q1}}^2 + 4\mu_{\mathrm{Q2}} & -\mu_{\mathrm{Q1}} \\ -\mu_{\mathrm{Q1}} & 2 \end{bmatrix} \\ \mathrm{P}_{Z_i} = \dfrac{1}{2}\begin{bmatrix} \mu_{\mathrm{D1}}^2 + 4\mu_{\mathrm{D2}} & -\mu_{\mathrm{D1}} \\ -\mu_{\mathrm{D1}} & 2 \end{bmatrix} \end{cases} \tag{29}$$

For simplicity, let us define $\|\gamma_\omega\|^{1/\delta_1} = |Z_\omega(t)| + {W_\omega}^{1/\delta_1}$ and $\|\gamma_i\|^{1/\delta_2} = |Z_i(t)| + W_i^{1/\delta_2}$. Thus, since the functions V_ω and

V_i are PD and RU, the following inequality set is satisfied:

$$\begin{cases} \lambda_{\min}\{P_{z_\omega}\}\|\gamma_\omega\|^{1/\delta_1} \le V_\omega \le \lambda_{\max}\{P_{z_\omega}\}\|\gamma_\omega\|^{1/\delta_1} \\ \lambda_{\min}\{P_{z_i}\}\|\gamma_i\|^{1/\delta_2} \le V_i \le \lambda_{\max}\{P_{z_i}\}\|\gamma_i\|^{1/\delta_2} \end{cases} \tag{30}$$

where $\lambda_{\min}\{\cdot\}$ and $\lambda_{\max}\{\cdot\}$ signify the least and largest eigenvalues, respectively. At this juncture, the derivatives of our possible Lyapunov functions V_ω and V_i can be respectively expressed as:

$$\begin{cases} \dot{V}_\omega = -\dfrac{1}{|Z_\omega(t)|^{\delta_1}}\left[\xi_\omega^T Q_{1Z_\omega}\xi_\omega - \dfrac{S_L}{K_T}\hat{U}_Q(t)Q_{2Z_\omega}{}^T\xi_\omega\right] \\ \dot{V}_i = -\dfrac{1}{|Z_i(t)|^{\delta_2}}\left[\xi_i^T Q_{1Z_i}\xi_i - S_L\hat{U}_D(t)Q_{2Z_i}{}^T\xi_i\right] \end{cases} \tag{31}$$

When we invoke *Assumption 2*, we can easily obtain:

$$\begin{cases} \dot{V}_\omega \le -\dfrac{1}{|Z_\omega(t)|^{\delta_1}}\xi_\omega^T Q_{Z_\omega}\xi_\omega \le \dfrac{1}{|Z_\omega(t)|^{\delta_1}}\lambda_{\min}\{Q_{z_\omega}\}\|\xi_\omega\|^{1/\delta_1} \\ \dot{V}_i \le -\dfrac{1}{|Z_i(t)|^{\delta_2}}\xi_i^T Q_{z_i}\xi_i \le \dfrac{1}{|Z_i(t)|^{\delta_2}}\lambda_{\min}\{Q_{z_i}\}\|\,\xi_i^{\xi}\,\big|^{1/\delta_2} \end{cases} \tag{32}$$

where

$$\begin{cases} Q_{Z_\omega} = \dfrac{\mu_{Q1}}{2} \\ \begin{bmatrix} \mu_{Q1}^2 + 2\mu_{Q2} - \left(\frac{4\mu_{Q2}}{\mu_{Q1}} + \mu_{Q1}\right)\mho_Q & -(\mu_{Q1} + 2\mho_Q) \\ -(\mu_{Q1} + 2\mho_Q) & 1 \end{bmatrix} \\ Q_{Z_i} = \dfrac{\mu_{D1}}{2} \\ \begin{bmatrix} \mu_{D1}^2 + 2\mu_{D2} - \left(\frac{4\mu_{D2}}{\mu_{D1}} + \mu_{D1}\right)\mho_D & -(\mu_{D1} + 2\mho_D) \\ -(\mu_{D1} + 2\mho_D) & 1 \end{bmatrix} \end{cases} \tag{33}$$

In the event that the super-twisting law gains are designed to satisfy Eq. (25), $Q_{Z_\omega} > 0$ and $Q_{Z_i} > 0$ (i.e., PD) are feasible by employing Eq. (28). Hence, $\dot{V}_\omega < 0$ and $\dot{V}_i < 0$ are achieved. Equation (32) can be referred to and the fact expressed as in Eq. (34):

$$\begin{cases} |Z_\omega(t)|^{\delta_1} \le \|\gamma_\omega\| \le \dfrac{V^{\delta_1}}{\lambda^{\delta_1}{}_{\min}\{P_{Z_\omega}\}};\ \|\gamma_\omega\| \ge \dfrac{V^{\delta_1}}{\lambda^{\delta_1}\max\{P_{z_\omega}\}} \\ |Z_i(t)|^{\delta_2} \le \|\gamma_i\| \le \dfrac{V^{\delta_2}}{\lambda^{\delta_2}{}_{\min}\{P_{z_i}\}};\quad \|\gamma_i\| \ge \dfrac{V^{\delta_2}}{\lambda^{\delta_2}{}_{\max}\{P_{z_i}\}} \end{cases} \tag{34}$$

to obtain Eq. (35):

$$\begin{cases} \dot{V}_\omega \le -\dfrac{\lambda_{\min}^{\delta_1}\{P_{Z_\omega}\}\lambda_{\min}\{Q_{Z_\omega}\}}{\lambda_{\max}\{P_{Z_\omega}\}}V^{\delta_1} \\ \dot{V}_i \le -\dfrac{\lambda_{\min}^{\delta_2}\{P_{Z_i}\}\lambda_{\min}\{Q_{Z_i}\}}{\lambda_{\max}\{P_{Z_i}\}}V^{\delta_2} \end{cases} \tag{35}$$

The expression just presented is an initial value problem whose solution we are after. To proceed, let us consider the case that the solution of the following initial value problem.

$$\begin{cases} \dot{v}_\omega(t) \le -c_\omega v_\omega^{\delta_1}(t); & v_\omega(t_0) = v_{\omega 0} \\ \dot{v}_i(t) \le -c_i v_i^{\delta_2}(t); & v_i(t_0) = v_{i0} \end{cases} \tag{36}$$

TABLE 2. Simulation parameters.

Parameter	Symbol
HOEDO (U_Q)	$N^q_1 = 15$; $N^q_2 = 75$; $N^q_3 = 125$
HOEDO (U_D)	$N^d_1 = 15$; $N^d_2 = 75$; $N^d_3 = 125$
SMC (V_q)	$\eta_1 = 500$; $\eta_2 = 2.5$; $\xi_\omega = 50$
ST-SMC (V_q)	$\mu_{D1} = 1$; $\mu_{D2} = 20$; $\delta_1 = 0.50$
SMC (V_d)	$\beta_1 = 1$; $\beta_2 = 1$; $\beta_{cc} = 1$
ST-SMC (V_d)	$\mu_{D1} = 1$; $\mu_{D2} = 25$; $\delta_2 = 0.50$
Others	$\rho = 1.25$; $A_w = 3$; $f_w = 0.0625$
	$C_{pmax} = 0.3262$; $\lambda_{opt} = 8.1$

is given by Eq. (32):

$$\left\{ v_\omega(t) = (v_{\omega 0}\delta_1 - \delta_1 c_\omega t)^{\frac{1}{\delta_1}} \quad ; \quad v_i(t) = (v_{i0}\delta_2 - \delta_2 c_i t)^{\frac{1}{\delta_2}} \right. \tag{37}$$

signifies that both $v_\omega(t)$ and $v_i(t)$ converge to zero within finite times $T_{s\omega}$ and T_{si} respectively given by:

$$\left\{ T_{s\omega} = \frac{v_\omega^{\delta_1}(t_0)}{\delta_1 c_\omega};\ T_{si} = \frac{v_i^{\delta_2}(t_0)}{\delta_2 c_i} \right. \tag{38}$$

By employing the theory of comparison of [50], it happens that $V_\omega(t) \le v_\omega(t)$ and $V_\omega(Z_{\omega 0}) \le v_{\omega 0}$. Similarly, $V_i(t) \le v_i(t)$ and $V_i(Z_{i0}) \le v_{i0}$. In this way, by invoking Eq. (37), $V_\omega(t)$ and $V_i(t)$ can be found, where c_ω and c_i in this context are presented as Eq. (39). Thus, $Z_\omega(t)$ and $Z_i(t)$ grasp the origin at most after finite times respectively expressed as in Eq. (40).

$$\begin{cases} c_\omega = \dfrac{\lambda^{\delta_1}\min\{P_{z_\omega}\}\lambda_{\min}\{Q_{z_\omega}\}}{\lambda_{\max}\{P_{Z_\omega}\}} \\ c_i = \dfrac{\lambda^{\delta_2}{}_{\min}\{P_{Z_i}\}\lambda_{\min}\{Q_{z_i}\}}{\lambda_{\max}\{P_{Z_i}\}} \end{cases} \tag{39}$$

$$\begin{cases} T_\omega = \dfrac{\lambda_{\max}\{P_{Z_\omega}\}}{\delta_1\lambda^{\delta_1}{}_{\min}\{P_{Z_\omega}\}\lambda_{\min}\{Q_{Z_\omega}\}}V^{\delta_1}(Z_{\omega 0}) \\ T_i = \dfrac{\lambda_{\max}\{P_{Z_i}\}}{\delta_2\lambda^{\delta_2}{}_{\min}\{P_{Z_i}\}\lambda_{\min}\{Q_{Z_i}\}}V^{\delta_2}(Z_{i0}) \end{cases} \tag{40}$$

Remark 2: In most studies, the controller and observer gains are selected using a trial-and-error approach. However, in this study, the parameters were chosen based on theoretical analysis, such as Lyapunov-based methods and estimation error convergence analysis. The controller and observer gains are presented in Table 2. The gains are selected according to Eqs. (14) and (25) to ensure stability and fast estimation convergence. Furthermore, the in-built optimization feature of MATLAB was used to obtain optimal gains while meeting the stability criteria. It is evident from the corresponding responses that effective shaft-speed tracking and uncertainty estimation were achieved.

VI. RESULTS AND ANALYSIS

To analyze the performance of the designed controllers and the proposed observer, the dynamic formulations of (6) for the PMSG-based WECS and the observer dynamics

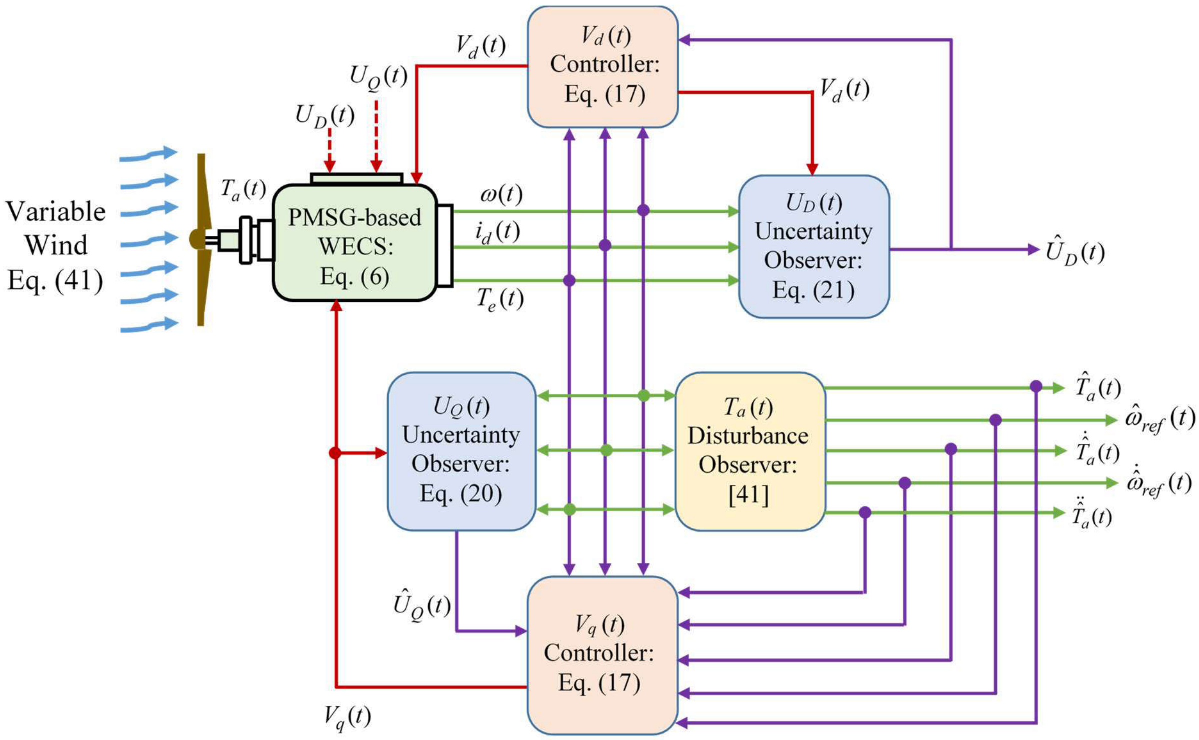

FIGURE 3. The block representation of HOEDO-based ST-SMC control of WECS with uncertainty estimation and compensation.

of (20) and (21) were simulated in the MATLAB environment, as illustrated in Fig. 3. It is worth noting that when the wind acts on the turbine blades, it creates an aerodynamic torque. However, the torque cannot be measured directly; thus, it is considered an external disturbance to be estimated by the observer. Thus, the observed $T_{\mathrm{a}}(t)$ and its auxiliary terms were fed to the controllers along with the observed parametric uncertainties related to the parameters of the PMSG. So, the controllers have prior knowledge of the uncertainties for better robustness and effective shaft-speed tracking.

The model parameters of Table 1 and the control gains of Table 2 were considered. The synthetic wind profile of Fig. 4, using the modified dynamics of (41), was used for the analysis, where A_w and f_w represent the amplitude and frequency of the wind profile, respectively. To further assess the performance of the controllers, the real wind profile from wind farm data, as shown in Fig. 4, was used for the validation. In all cases, the simulation analysis was conducted for 100 seconds to allow for a comprehensive analysis of the control system.

$$v(t) = A_w \begin{pmatrix} 10 + 0.55\left(\sin(0.2\pi f_w t) - 0.875\sin(0.6\pi f_w t)\right. \\ +0.75\sin(\pi f_w t) - 0.625\sin(2\pi f_w t) \\ -0.5\sin(6\pi f_w t) + 0.25\sin(10\pi f_w t) \\ \left. +0.125\sin(20\pi f_w t)\right) \end{pmatrix} \tag{41}$$

A. SHAFT SPEED TRACKING UNDER PARAMETRIC UNCERTAINTIES

Figure 4 shows the response of the aerodynamic torque and its estimation using the HOEDO. As illustrated, the torque was estimated satisfactorily as it followed the desired torque well. This torque estimation was then incorporated into the controllers to generate appropriate control signals for the WECS, as illustrated in (13) and (14). In addition, the response of the parametric uncertainty estimation for $\mathrm{U_D}(t)$ and $\mathrm{U_Q}(t)$ was illustrated in Fig. 4 for the combined uncertainties of resistance and inductance in the d and q axes, respectively. In both cases, the estimation was satisfactory.

B. DISTURBANCE AND PARAMETRIC UNCERTAINTY ESTIMATIONS

Herein, the performance of the two controllers is investigated in terms of tracking errors under different operating scenarios. Thus, the main objective of the work is to achieve precise speed tracking of the generator for maximum power harnessing of the wind source. The following three scenarios were analyzed for a comprehensive assessment of the designed controller's performance:

Case 1: The speed tracking is analyzed using the nominal values of the PSMG-based WECS of Table 1 and the formulation of (6) without any uncertainty. Thus, the ideal behavior of the control system will be investigated.

Case 2: In this case, the three parametric uncertainties relating to system parameters, namely, resistance and inductance, i.e. $\mathrm{U_Q}(t)$ and $\mathrm{U_D}(t)$ of (16), were considered. These

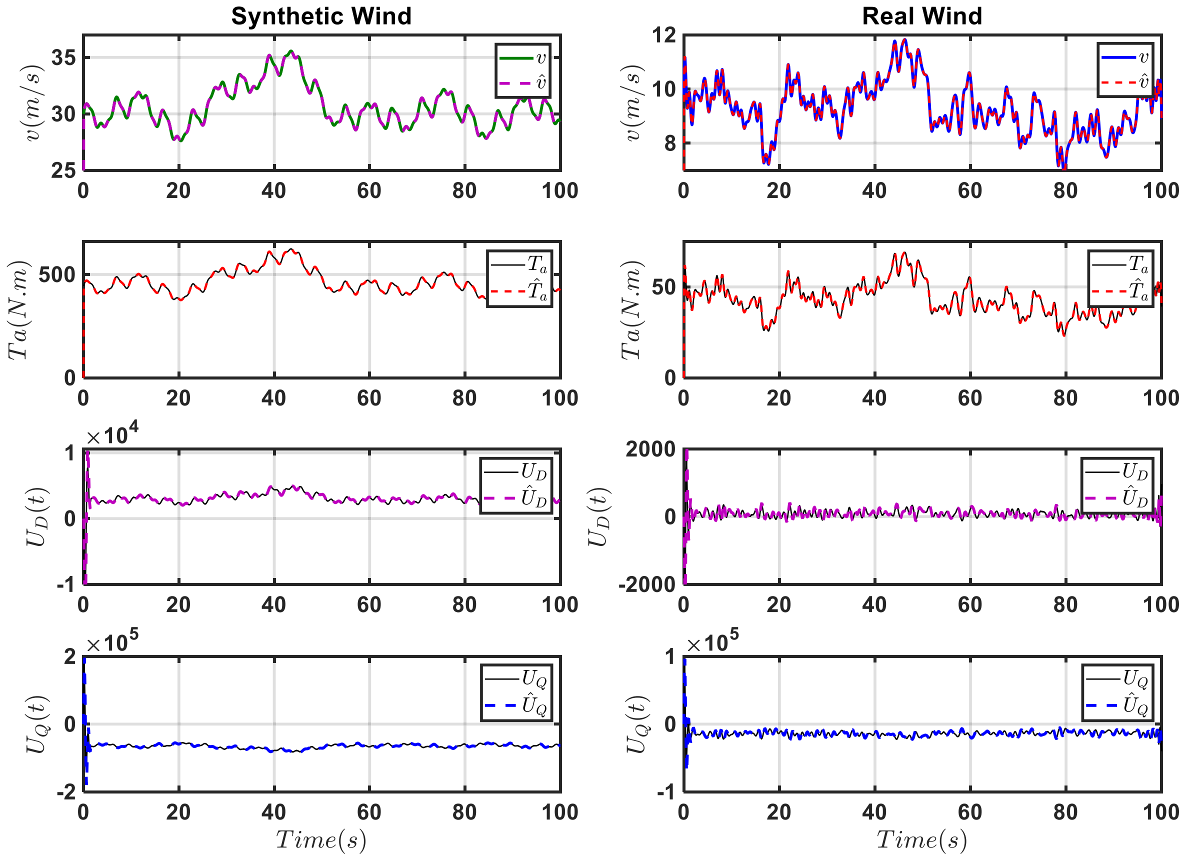

FIGURE 4. The estimation performance of the designed observers for wind speed (v), aerodynamic torque (T_a), and parametric uncertainties (U_D and U_Q) using synthetic and real-wind data. In both cases, the wind speed and the disturbances were estimated satisfactorily.

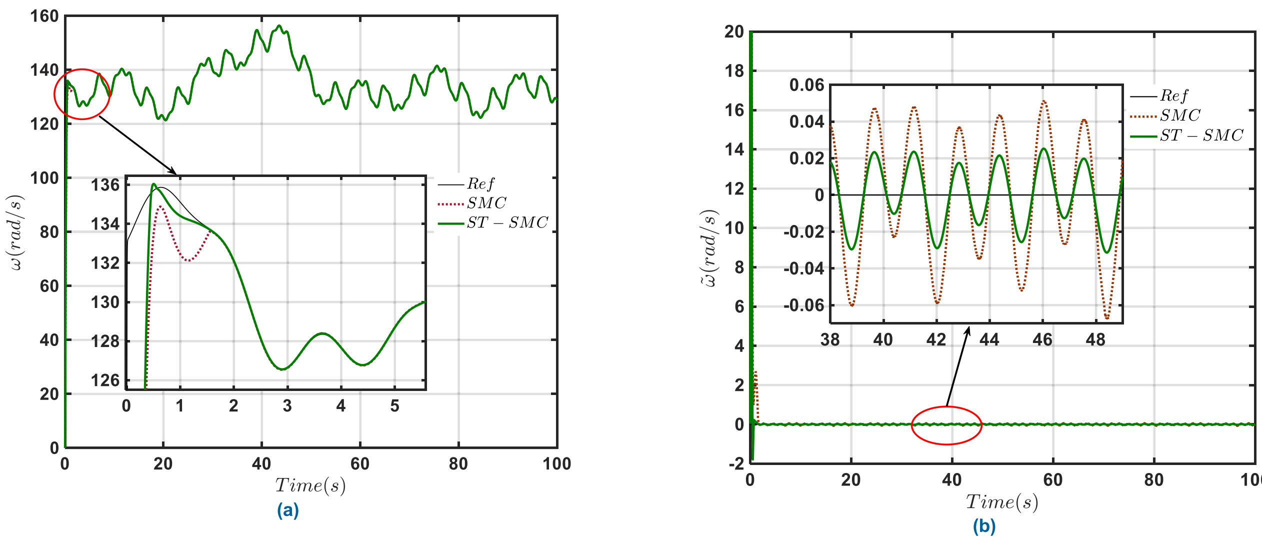

FIGURE 5. The Performance of SMC and ST-SMC with PMSG's nominal values without any uncertainty (Case 1); (a) Speed tracking; (b) Tracking error (ω-ω_{ref}).

parameters were chosen because they will inevitably change from their nominal values after long-term operation. Thus, the nominal resistance was increased by 50%, whereas the inductance was decreased by 2%. Therefore, the controller's robustness would be tested in the presence of these parametric uncertainties. Hence, the reliability of the control scheme will be tested and analyzed.

Case 3: Here, the disturbance rejection mechanism is incorporated into the controllers such that the uncertainty compensation is part of the controllers, as shown in (17).

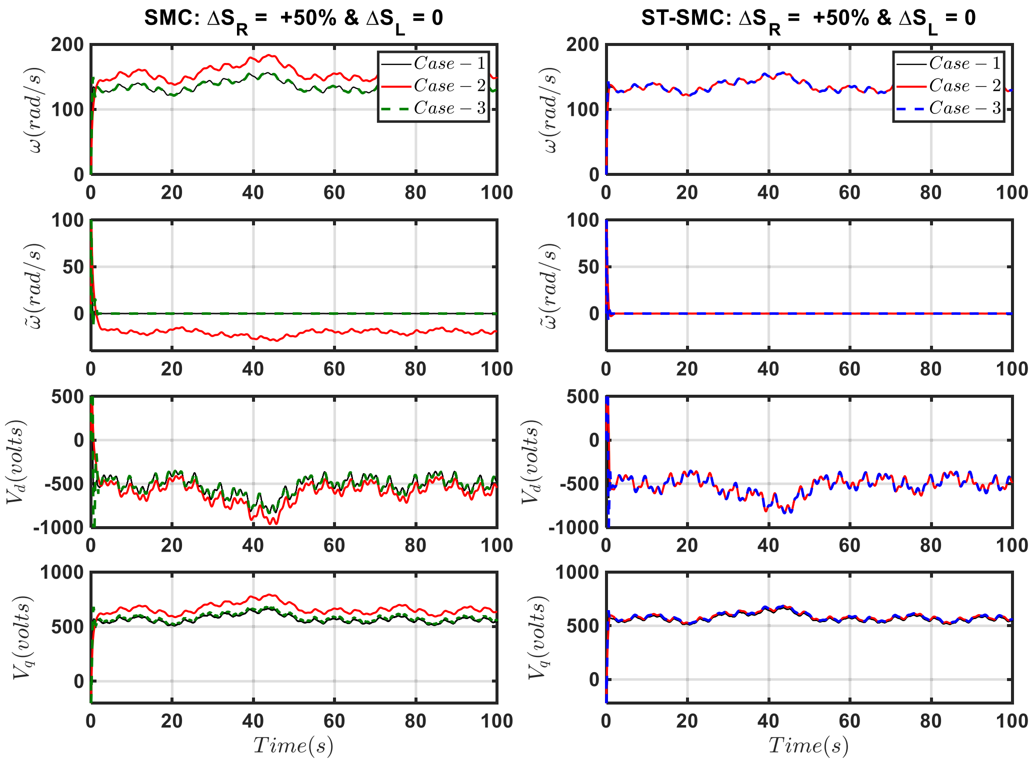

FIGURE 6. Performance of SMC and ST-SMC for the three cases with only changes of stator resistance ($\Delta S_R = +50\%$) using synthetic wind profile. It is obvious that the changes in resistance affect the performance of SMC, but the impact was satisfactorily compensated for using the disturbance observers (case 3). On the one hand, the ST-SMC demonstrates inherent robustness to the associated uncertainty.

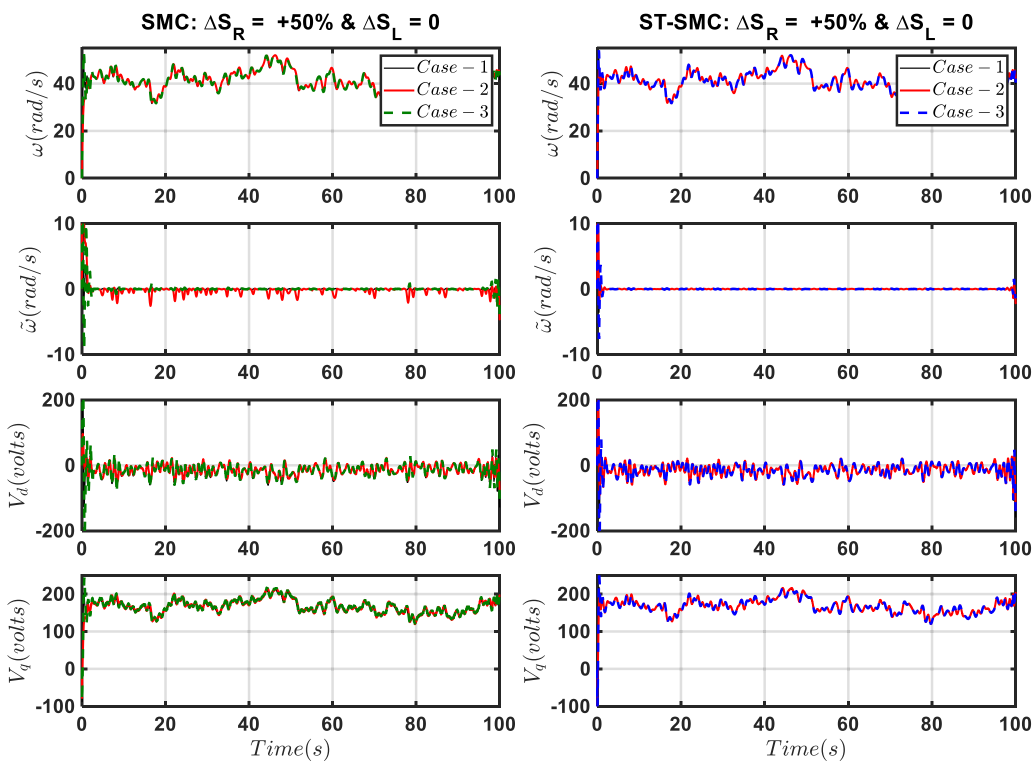

FIGURE 7. Performance of SMC and ST-SMC for the three cases with only changes of stator resistance ($\Delta S_R = +50\%$) using real wind profile. It is obvious that the changes in resistance affect the performance of SMC, but the impact was satisfactorily compensated for using the disturbance observers (case 3). On the one hand, the ST-SMC demonstrates inherent robustness to the associated uncertainty.

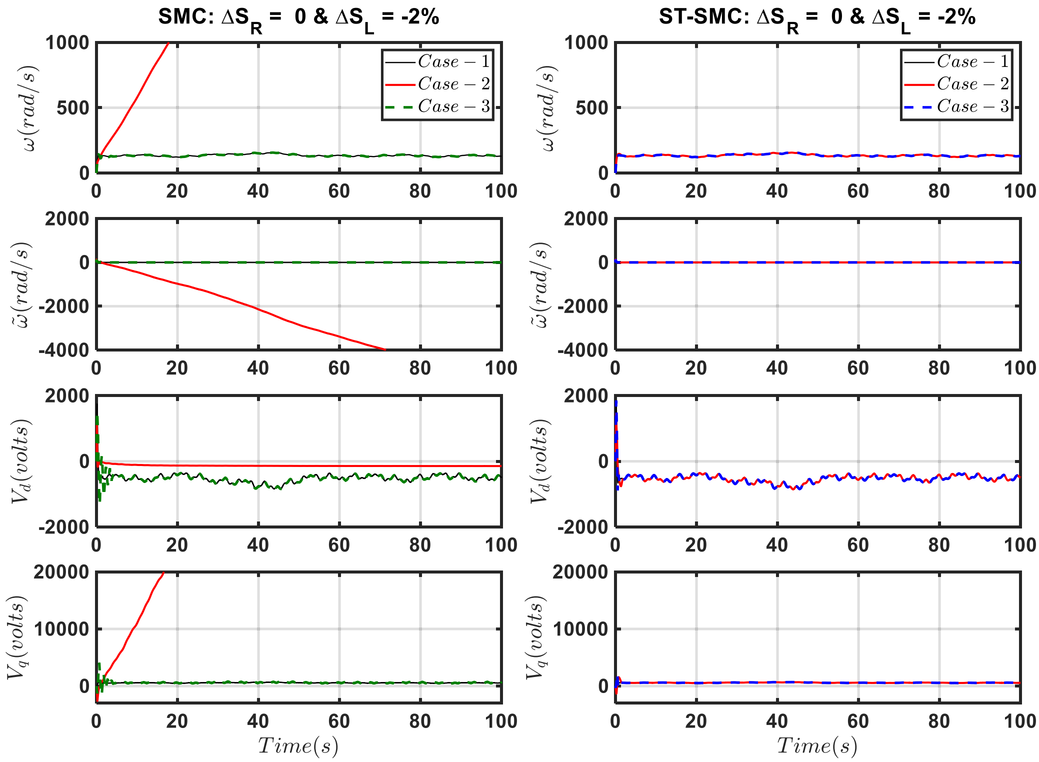

FIGURE 8. Performance of SMC and ST-SMC for the three cases with only changes of stator inductance ($\Delta S_L = -2\%$) using synthetic wind profile. The changes in inductance caused the SMC to be unstable, but the impact was satisfactorily compensated using the disturbance observers (case 3). On the one hand, the ST-SMC demonstrates inherent robustness to the associated uncertainty.

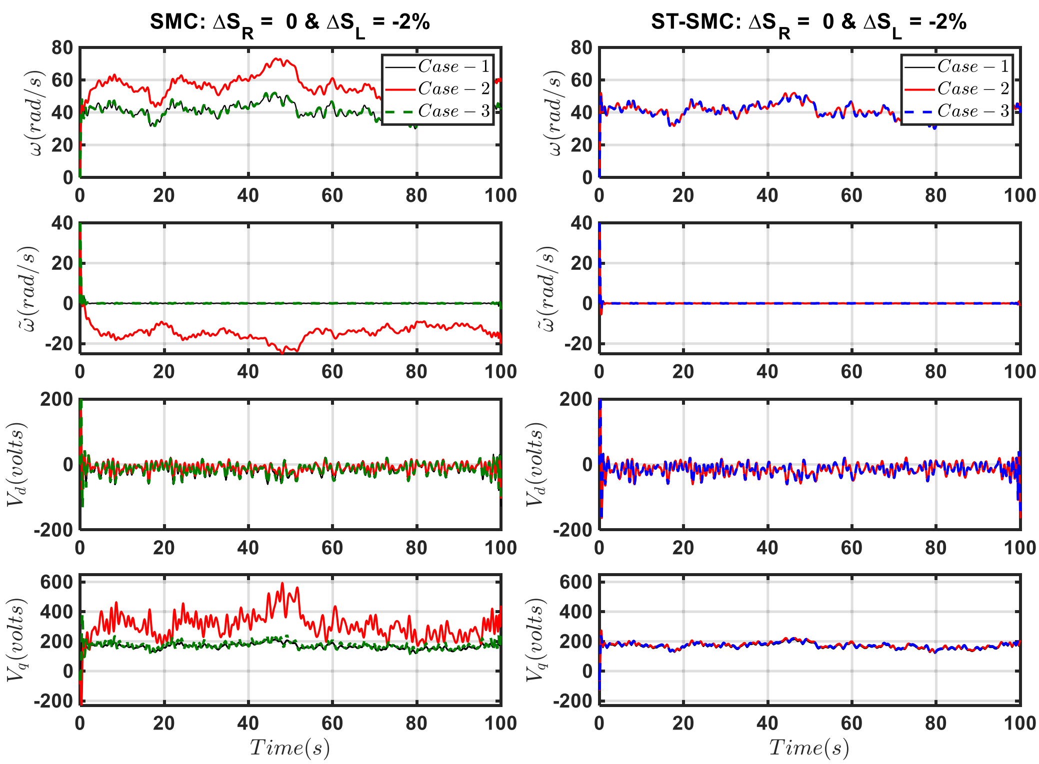

FIGURE 9. Performance of SMC and ST-SMC for the three cases with only changes of stator inductance ($\Delta S_L = -2\%$) using real wind data. The changes in inductance affect the SMC significantly, but the impact was satisfactorily compensated for using the disturbance observers (case 3). On the one hand, the ST-SMC demonstrates inherent robustness to the associated uncertainty.

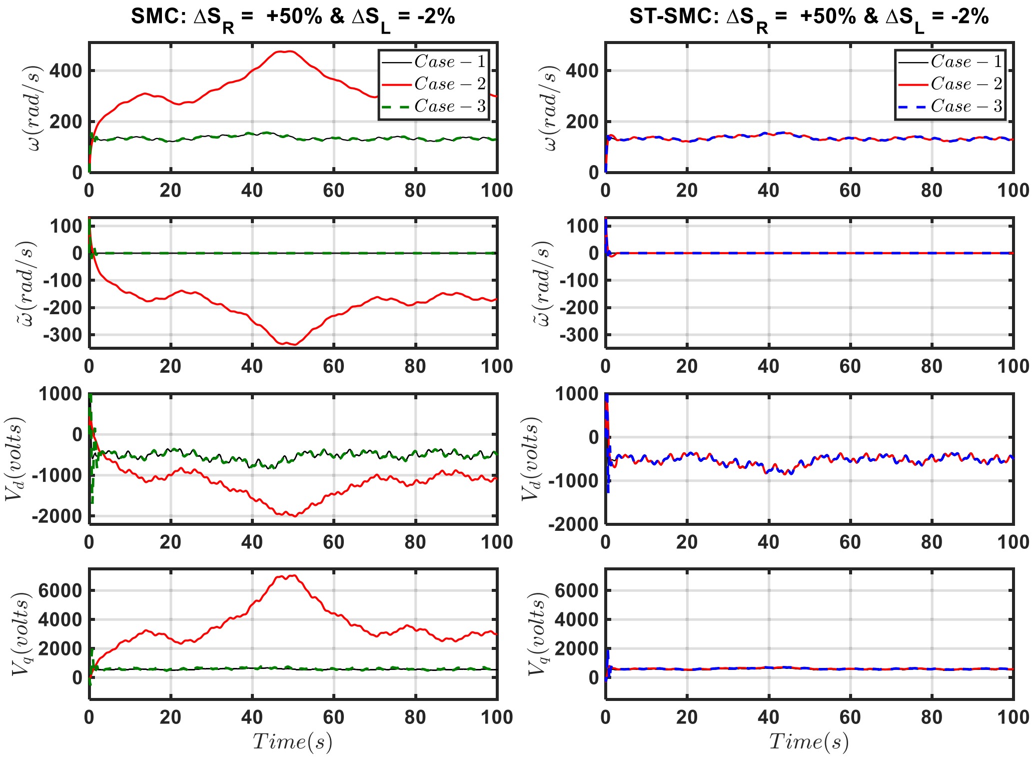

FIGURE 10. The performance of SMC and ST-SMC for the three cases with simultaneous changes in stator resistance and inductance ($\Delta SR = +50\%$ and $\Delta SL = -2\%$) using synthetic wind profile. The combined changes affect the SMC significantly, but the impact was satisfactorily compensated using the disturbance observers (case 3). On the one hand, the ST-SMC demonstrates inherent robustness to the combined uncertainties.

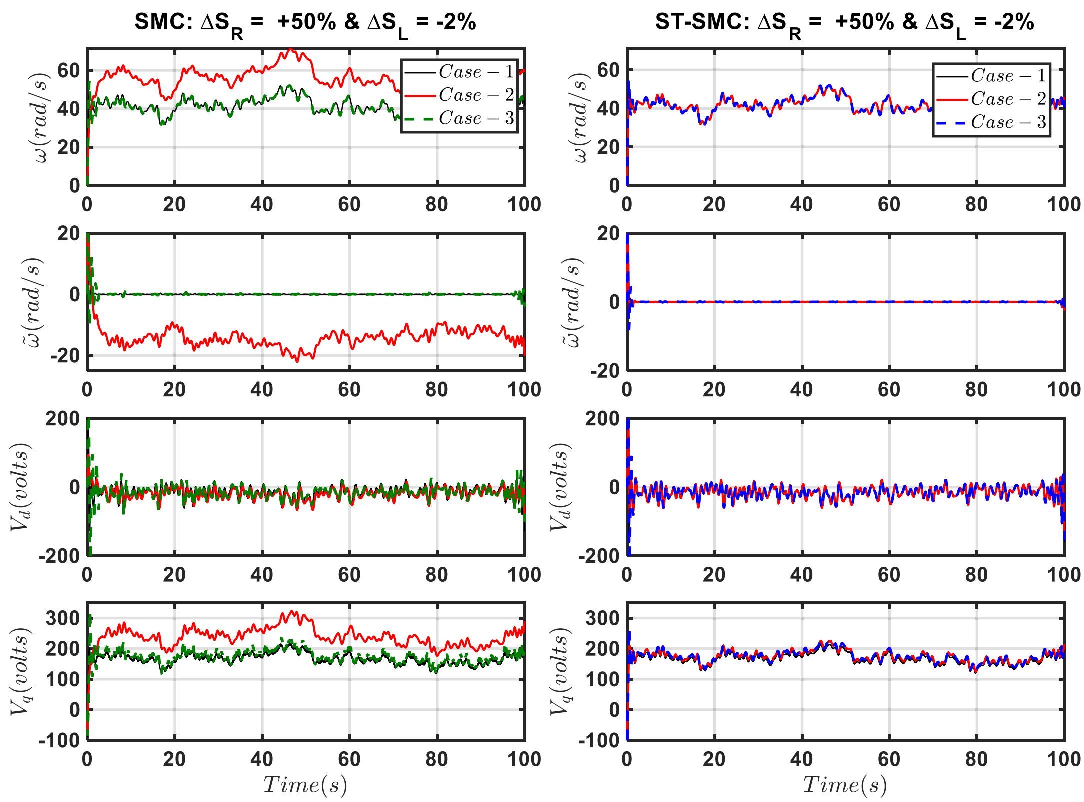

FIGURE 11. The performance of SMC and ST-SMC for the three cases with simultaneous changes in stator resistance and inductance ($\Delta SR = +50\%$ and $\Delta SL = -2\%$) using real wind data. The combined changes affect the SMC significantly, but the impact was satisfactorily compensated using the disturbance observers (case 3). On the one hand, the ST-SMC demonstrates inherent robustness to the combined uncertainties.

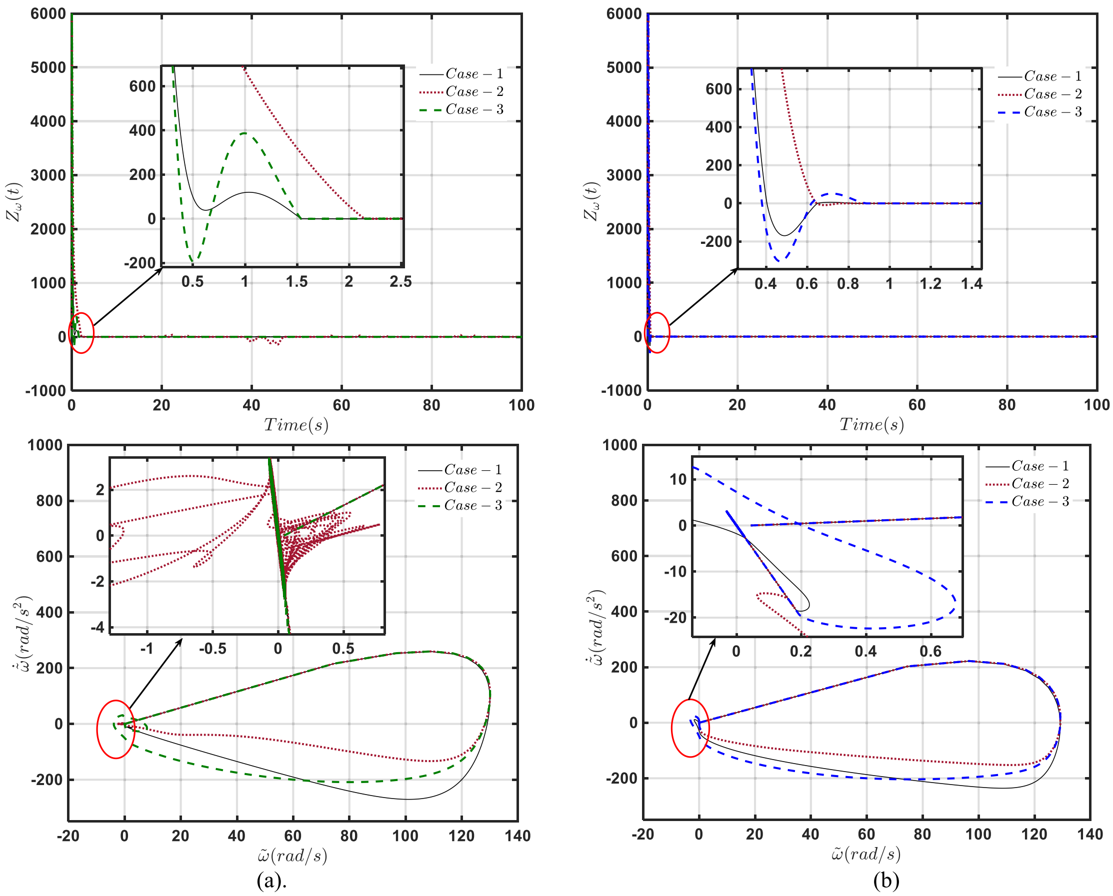

FIGURE 12. Implementation of the SMC and ST-SMC with the change of stator resistance (ΔSR = +20%); (a) Trajectory of the sliding surface for SMC; (b) Trajectory of the sliding surface for ST-SMC. The STMC drove the states to their origins and stayed there, unlike the SMC, which caused visible chattering at the origin.

Thus, the controllers' ability to compensate for the uncertainties would be assessed.

Figure 5(a) shows the response of the speed control performance for the nominal values of the system without any uncertainties using the synthetic wind profile of Fig. 4. The corresponding tracking error demonstrated that the ST-SMC within error within ± 0.02 rad/s has better tracking performance compared to the traditional SMC, with an error within ± 0.06 rad/s, as shown in Fig. 5(b). Moreover, the ω(t) tracking performance, corresponding tracking errors, and the control signals V_q(t) and V_d(t) for each of the three cases are presented in Figs. 6-11. The results demonstrate the effectiveness of the ST-SMC even in the presence of unknown disturbance. On the other hand, the SMC's performance deteriorates in the presence of disturbance (Case - 2). Moreover, the control was validated using real wind data from a wind farm, and the corresponding responses were presented. As shown, the performance of the control followed a similar pattern to that of the synthetic wind response, where the ST-SMC demonstrated superior performance. Finally, the control V_q(t) and V_d(t) for each control were analyzed for the two different wind profiles, as shown. It is worth noting that the SMC exhibits a lot of chattering effects, which would adversely affect the actuation in practical implementations.

Remark 3: The estimation error is the primary metric for evaluating DOB performance. As shown in Fig. 4, the proposed HOEDO achieves a minimal error of 0.05 N·m in torque estimation, significantly outperforming the generalized disturbance observer (GDO) [51], generalized high-order disturbance observer (GHODO) [52], and high-order optimal disturbance observer (HOODO) [39], which reported errors as high as 0.6273 N·m. This demonstrates HOEDO's superior estimation, enabling improved shaft-speed tracking, and better energy harnessing.

C. DISCUSSIONS

As earlier stated, unmatched disturbances, including parametric uncertainties, were complex for the SMC to handle. Figure 13 (a)-(b) shows the typical implementation of the SMC and ST-SMC algorithms. The control mechanism forced the states of interest to follow the predefined trajectory from the initial position to the final desired position (origin). However, chattering generally occurs on the sliding surface using the traditional SMC, which is mitigated using the advanced ST-SMC. This process can be clearly identified where the SMC struggles to settle at the original, particularly in the presence of uncertainties (Case 2), as compared to the ST-SMC.

TABLE 3. Summary of shaft speed tracking perfromance of the SMC AND ST-SMC using synthetic and real wind profiles.

Index		Scenarios	Synthetic wind profile				Real-wind profile			
			Transient response (0 – 10 sec)		Steady-state response (10 – 100 sec)		Transient response (0 – 10 sec)		Overall response (0 – 100 sec)	
			SMC	STSMC	SMC	STSMC	SMC	STSMC	SMC	STSMC
Case 1	MAE	Nominal (ΔS_R & ΔS_L = 0%)	2.3143	2.0245	0.2577	0.2150	0.9181	0.6661	0.1480	0.0942
	RMSE	Nominal (ΔS_R & ΔS_L = 0%)	12.8328	12.5917	4.0584	3.9820	4.4902	3.9082	1.4238	1.2372
Case 2	MAE	ΔS_R = +50% & ΔS_L = 0%	19.7502	3.4250	20.3791	0.3550	2.1460	0.9084	0.4415	0.1215
		ΔS_R = 0% & ΔS_L = -2%	202.1211	3.0486	2749.9	0.3174	13.2336	0.7322	14.5003	0.1012
		ΔS_R = +50% & ΔS_L = -2%	98.2660	4.7944	191.4264	0.4920	13.6373	0.9565	14.2984	0.1275
	RMSE	ΔS_R = +50% & ΔS_L = 0%	24.3880	15.5057	21.0741	4.9036	6.5006	4.7782	2.1074	1.5135
		ΔS_R = 0% & ΔS_L = -2%	240.7894	13.2635	3215.4	4.1945	14.3477	4.0013	14.9321	1.2667
		ΔS_R = +50% & ΔS_L = -2%	106.0253	16.0576	201.3098	5.0781	14.7373	4.8381	14.6049	1.5328
Case 3	MAE	ΔS_R = +50% & ΔS_L = 0%	3.3618	2.3231	0.3623	0.2448	1.6647	0.9186	0.2449	0.1223
		ΔS_R = 0% & ΔS_L = -2%	4.1793	2.0254	0.4434	0.2151	1.0153	0.6687	0.1593	0.0946
		ΔS_R = +50% & ΔS_L = -2%	4.2594	2.5141	0.4524	0.2639	1.9007	0.9585	0.2741	0.1268
	RMSE	ΔS_R = +50% & ΔS_L = 0%	14.4909	13.4270	4.5827	4.2462	5.4319	4.3761	1.7308	1.3866
		ΔS_R = 0% & ΔS_L = -2%	13.8691	12.6026	4.3861	3.9855	4.5690	3.9236	1.4497	1.2421
		ΔS_R = +50% & ΔS_L = -2%	15.2429	13.5275	4.8206	4.2780	5.6663	4.4309	1.8078	1.4043

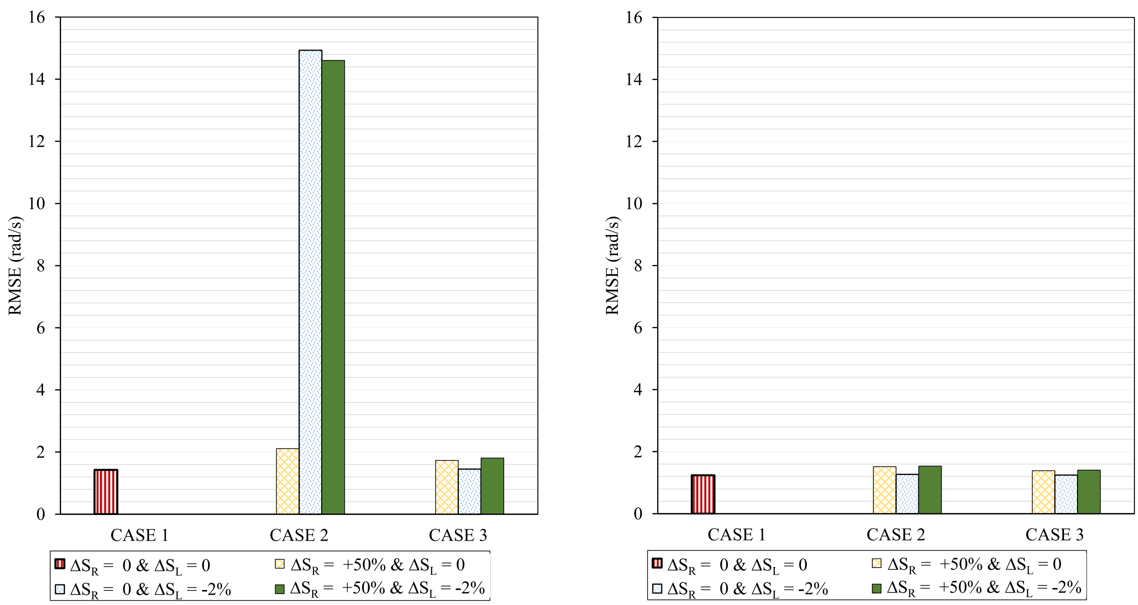

FIGURE 13. The RMSE of the overall response (0 – 100 sec) of the speed tracking using the real-wind data; (a) Although the SMC was ineffective in rejecting the uncertainties, the compensation mechanism (case 3) significantly rejects the parametric uncertainties (case 2); (b) The ST-SMC demonstrates strong robustness to parametric uncertainties as compared to its performance without the uncertainties (Case 1). A slight improvement can be observed using the compensation mechanism for the ST-SMC (Case 3).

In the preceding sections, the SMC and ST-SMC algorithms were analyzed according to their ability to handle uncertainties and unmatched disturbances. The disturbance compensation performance was investigated using three different cases. Firstly, the controllers' performance was compared without changing the system parameters (Case 1), i.e., using nominal plant dynamics. Then, the unmatched disturbance was introduced to the system by changing the stator resistance and inductance value by some percentage. Finally, the compensation scheme was designed using the disturbance observers. In each case, the control performance using the synthetic wind and the real wind data from a wind farm were analyzed. Table 3 Summarized the overall performance of the controllers using two popular performance indices, namely, root mean square error (RMSE) and mean absolute error (MAE) of the speed tracking (ω-ω_{ref}). To have a better comparative analysis, the transient response (0-10 sec) and the overall response (0-100 sec) were analyzed.

Although the RMSE is generally higher than the MAE, both describe the deviation between the reference and actual signals. Low values indicate more accurate control performance in each case and vice versa. Table 3 shows that both MAE and RMSE have a similar pattern. Thus, to clearly demonstrate the effectiveness of controllers, the visualization of the summarized results of Table 3 is presented using the RMSE of real-wind data. As shown in Fig. 12(a), the response of SMC without compensation (case 2) is ineffective as it deviates significantly from the original response (case 1) of 1.42 rad/s to 14.93 rad/s when the stator inductance was changed. However, the control was not much affected when only the resistance changed (2.11 rad/s). Nonetheless, the compensation mechanism (case 3) shows the effectiveness of the parametric uncertainty estimation and compensation. On the other hand, Fig. 12(b) demonstrates the superior inherent uncertainty rejection of the ST-SMC, demonstrating a little deviation from the original response (case 1) of 1.24 rad/s to 1.53 rad/s compared to SMC.

In summary, the analyses demonstrated that the compensation mechanisms using uncertainty estimation could improve the speed-tracking performance of the wind turbine generator, particularly for the traditional SMC. Although the performance of the ST-SMC was enhanced slightly, its inherent robustness can effectively reject the parametric uncertainties associated with the changes in stator inductance and resistance of the generator. Thus, the ST-SMC not only minimizes the chattering problem of the SMC but also improves its robustness to parametric uncertainties.

VII. CONCLUSION AND FUTURE WORK

This study investigates the impact of the generator's parametric uncertainties due to changes in stator resistance and inductance on the shaft speed tracking of WECS using SMC and ST-SMC algorithms. The uncertainties were expressed as a lumped disturbance and effectively estimated using the concept of disturbance estimation. The controllers demonstrated significant speed tracking when the nominal parameters of the WECS were used. However, the performance of the traditional SMC was significantly affected when the uncertainties were introduced. Remarkably, the performance was greatly improved when the compensation mechanism was incorporated into the control scheme. The overall response of the controllers using the speed tracking error performance indices (RMSE and MAE) shows that the advanced ST-SMC has superior robustness to parametric uncertainties as compared to the traditional SMC. The analyses show that the proposed scheme could be satisfactorily applied for sensorless wind speed estimation and control of the turbine's shaft speed for optimal harnessing of wind energy, even in the presence of inevitable parametric uncertainties. Finally, this research focuses on the turbine-generator side of the WECS. However, the grid is often characterized by voltage fluctuations and harmonic distortion due to different loading conditions. Therefore, the possible application of the DOB-based ST-SMC for grid integration would be the focus of our future work.

Moreover, the study validated the control method using simulation studies, limiting generalizability. Future work should implement the study in hardware-in-the-loop setups for further practical insights.

DECLARATION OF COMPETING INTEREST

The authors declare that they have no known competing financial interests or personal relationships that could have appeared to influence the work reported in this article.

REFERENCES

[1] V. Tamilselvan, S. S. Subramanian, and V. D. Kumar, "Hybrid approach for 3 phase bridgeless AC to DC Cuk converter for WECS," *Int. J. Electron.*, pp. 1–27, Feb. 2024, doi: 10.1080/00207217.2024.2312559.

[2] M. Yessef, H. Benbouhenni, M. Taoussi, A. Lagrioui, I. Colak, B. Bossoufi, and T. A. H. Alghamdi, "Experimental validation of feedback PI controllers for multi-rotor wind energy conversion systems," *IEEE Access*, vol. 12, pp. 7071–7088, 2024, doi: 10.1109/ACCESS.2024.3351355.

[3] A. Mseddi, A. Abid, O. Naifar, M. Rhaima, A. B. Makhlouf, and L. Mchiri, "Harnessing the potential of high-efficiency synchronous generators in wind energy conversion systems," *IEEE Access*, vol. 12, pp. 58871–58886, 2024, doi: 10.1109/ACCESS.2024.3379272.

[4] GWEC. (2023). *Global Wind Report 2023*. [Online]. Available: http://www.gwec.net/global-figures/wind-energy-global-status/

[5] Y. Kazemi and M. M. Rezaei, "A grid forming control for wind energy conversion systems," *Energy Rep.*, vol. 9, pp. 2016–2026, Dec. 2023, doi: 10.1016/j.egyr.2023.01.037.

[6] A. Sotoudeh and M. M. Rezaei, "An adaptive control strategy for grid-forming of SCIG-based wind energy conversion systems," *Energy Rep.*, vol. 10, pp. 114–122, Nov. 2023, doi: 10.1016/j.egyr.2023.06.030.

[7] S. Tyagi, B. Singh, and S. Das, "Seamless connection of wind and small hydro based energy conversion system with storage," *IEEE Trans. Ind. Appl.*, vol. 60, no. 3, pp. 4292–4301, May 2024, doi: 10.1109/TIA.2024.3351114.

[8] M. S. Dall'Asta and T. B. Lazzarin, "A review of fast power-reserve control techniques in grid-connected wind energy conversion systems," *Energies*, vol. 17, no. 2, p. 451, Jan. 2024, doi: 10.3390/en17020451.

[9] M. P. Selvam, S. K. Palraj, and G. S. Madasamy, "Adaptive control of a single source reduced switch MLI-based DSTATCOM for wind energy conversion system," *Electr. Eng.*, vol. 106, no. 5, pp. 5269–5290, Jan. 2024, doi: 10.1007/s00202-023-02201-x.

[10] V. R. Rosales-Valladares, N. M. Salgado-Herrera, O. Rodríguez-Hernández, J. R. Rodríguez-Rodríguez, D. Granados-Lieberman, and O. Anaya-Lara, "Power hardware in the loop methodology applied in the integration of wind energy conversion system under fluctuations: A case study," *Energy Sources A, Recovery, Utilization, Environ. Effects*, vol. 46, no. 1, pp. 2767–2791, Dec. 2024, doi: 10.1080/15567036.2024.2308646.

[11] R. Saulescu, C. Jaliu, M. Neagoe, D. Ciobanu, and N. Cretescu, "Comparative analysis of torque-adding wind energy conversion systems with a counter-rotating vs. conventional electric generator," *Frontiers Energy Res.*, vol. 11, p. 1, Aug. 2023, doi: 10.3389/fenrg.2023.1215509.

[12] M. A. Mostafa, E. A. El-Hay, and M. M. Elkholy, "An overview and case study of recent low voltage ride through methods for wind energy conversion system," *Renew. Sustain. Energy Rev.*, vol. 183, Sep. 2023, Art. no. 113521, doi: 10.1016/j.rser.2023.113521.

[13] A. Chaudhuri, R. Datta, M. P. Kumar, J. P. Davim, and S. Pramanik, "Energy conversion strategies for wind energy system: Electrical, mechanical and material aspects," *Materials*, vol. 15, no. 3, p. 1232, Feb. 2022, doi: 10.3390/ma15031232.

[14] I. Lopez-Garcia, C. S. Lopez-Monsalvo, O. Gomez-Gonzalez, M. Sanabria-Villamizar, F. Beltran-Carbajal, and R. Escarela-Perez, "On the regulation of wind energy conversion systems working as conventional generation plants," *Mathematics*, vol. 11, no. 11, p. 2495, May 2023, doi: 10.3390/math11112495.

[15] J. Li, G. Wang, Z. Li, S. Yang, W. T. Chong, and X. Xiang, "A review on development of offshore wind energy conversion system," *Int. J. Energy Res.*, vol. 44, no. 12, pp. 9283–9297, Oct. 2020, doi: 10.1002/er.5751.

[16] B. P. Ganthia, S. K. Barik, and B. Nayak, "Wind turbines in energy conversion system: Types & techniques," in *Renewable Energy and Future Power Systems* (Energy Systems in Electrical Engineering), V. K. Singh, A. K. Bhoi, A. Saxena, A. F. Zobaa, and S. Biswal, Eds., Singapore: Springer, 2021, pp. 199–217, doi: 10.1007/978-981-33-6753-1_9.

[17] P. A. Hosseinabadi, H. Pota, S. Mekhilef, and H. Schwartz, "Fixed-time observer-based control of DFIG-based wind energy conversion systems for maximum power extraction," *Int. J. Electr. Power Energy Syst.*, vol. 146, Mar. 2023, Art. no. 108741, doi: 10.1016/j.ijepes.2022.108741.

[18] A. S. S. Vardhan and U. K. Sinha, "Control strategies and performance analysis of doubly fed induction generator for grid-connected wind energy conversion system," *Electr. Eng.*, vol. 106, no. 2, pp. 1203–1224, Apr. 2024, doi: 10.1007/s00202-023-02079-9.

[19] Y. Mousavi, G. Bevan, I. B. Kucukdemiral, and A. Fekih, "Observer-based high-order sliding mode control of DFIG-based wind energy conversion systems subjected to sensor faults," *IEEE Trans. Ind. Appl.*, vol. 60, no. 1, pp. 1750–1759, Jan. 2024, doi: 10.1109/TIA.2023.3317823.

[20] Y. Dong, J. Wang, S. Ding, and W. Li, "Adaptive fractional-order fault-tolerant sliding mode control scheme of DFIG wind energy conversion system," *Proc. Inst. Mech. Eng. I, J. Syst. Control Eng.*, vol. 237, no. 1, pp. 15–25, Jan. 2023, doi: 10.1177/09596518221123101.

[21] S. S. Rauth, D. Kastha, and P. Bajpai, "A sensorless control strategy for automatic start-up and grid-synchronization of doubly fed induction generator in wind energy conversion system," *Int. J. Circuit Theory Appl.*, vol. 52, no. 4, pp. 1733–1753, Apr. 2024, doi: 10.1002/cta.3843.

[22] W. S. E. Abdellatif, A. A. Elsakaan, A. F. Barakat, and N. A. Nouraldin, "A comparative performance analysis of DFIG and PMSG-based WECS," in *Proc. 23rd Int. Middle East Power Syst. Conf. (MEPCON)*, Dec. 2022, pp. 1–6, doi: 10.1109/MEPCON55441.2022.10021738.

[23] M. Eldoromi, D. Fateh, M. Rostamzade, and A. A. M. Birjandi, "PMSG and DFIG-based wind energy conversion systems," in *Power Electronics for Next-Generation Drives and Energy Systems. Volume 2: Clean Generation and Power Grids*. Stevenage, U.K.: Institution of Engineering and Technology (IET), 2022, pp. 67–89, doi: 10.1049/PBPO207G_ch4.

[24] X. Yang, J. Yao, and W. Deng, "Output feedback adaptive super-twisting sliding mode control of hydraulic systems with disturbance compensation," *ISA Trans.*, vol. 109, pp. 175–185, Mar. 2021, doi: 10.1016/j.isatra.2020.09.014.

[25] X. Yang, W. Deng, and J. Yao, "Disturbance-observer-based adaptive command filtered control for uncertain nonlinear systems," *ISA Trans.*, vol. 130, pp. 490–499, Nov. 2022, doi: 10.1016/j.isatra.2022.04.007.

[26] S. Sumbekov, B. D. H. Phuc, and T. D. Do, "Takagi–Sugeno fuzzy-based integral sliding mode control for wind energy conversion systems with disturbance observer," *Electr. Eng.*, vol. 102, no. 3, pp. 1141–1151, Sep. 2020, doi: 10.1007/s00202-020-00939-2.

[27] B. Torchani, A. T. Azar, S. Ahmed, A. R. Mahlous, and I. K. Ibraheem, "Sliding mode control based on maximum power point tracking for dynamics of wind turbine system," *Frontiers Energy Res.*, vol. 12, Aug. 2024, Art. no. 1434695, doi: 10.3389/fenrg.2024.1434695.

[28] L.-G. Hua, A. Ali, S. Ullah, G. Hafeez, M. M. Zaidi, and L. J. Jun, "Robust finite-time integral terminal sliding mode control design for maximum power extraction of PMSG-based standalone wind energy system," *Frontiers Energy Res.*, vol. 11, Nov. 2023, Art. no. 1293267, doi: 10.3389/fenrg.2023.1293267.

[29] Z. Zhang and X. Liu, "An improved super-twisting sliding mode single-loop control with current-constraint for PMSM based on two-time scale disturbance observer," *IEEE Trans. Transport. Electrific.*, vol. 10, no. 3, pp. 5389–5399, Sep. 2024, doi: 10.1109/TTE.2023.3322687.

[30] Z. Zhang, X. Liu, J. Yu, and H. Yu, "Time-varying disturbance observer based improved sliding mode single-loop control of PMSM drives with a hybrid reaching law," *IEEE Trans. Energy Convers.*, vol. 38, no. 4, pp. 2539–2549, Dec. 2023, doi: 10.1109/TEC.2023.3277628.

[31] D. Wang, S. Liu, X. Liu, Z. Zhang, and Y. Chen, "Improved model–free sliding mode control of PMSM based on finite-time generalized proportional integral observer," in *Proc. IEEE 12th Data Driven Control Learn. Syst. Conf. (DDCLS)*, Xiangtan, China, May 2023, pp. 501–505, doi: 10.1109/DDCLS58216.2023.10166026.

[32] S. M. Mozayan, M. Saad, H. Vahedi, H. Fortin-Blanchette, and M. Soltani, "Sliding mode control of PMSG wind turbine based on enhanced exponential reaching law," *IEEE Trans. Ind. Electron.*, vol. 63, no. 10, pp. 6148–6159, Oct. 2016, doi: 10.1109/TIE.2016.2570718.

[33] Y. Mousavi, G. Bevan, I. B. Kucukdemiral, and A. Fekih, "Sliding mode control of wind energy conversion systems: Trends and applications," *Renew. Sustain. Energy Rev.*, vol. 167, Oct. 2022, Art. no. 112734, doi: 10.1016/j.rser.2022.112734.

[34] L. Hu, F. Xue, Z. Qin, J. Shi, W. Qiao, W. Yang, and T. Yang, "Sliding mode extremum seeking control based on improved invasive weed optimization for MPPT in wind energy conversion system," *Appl. Energy*, vol. 248, pp. 567–575, Aug. 2019, doi: 10.1016/j.apenergy.2019.04.073.

[35] L. C. Pagnini, M. Burlando, and M. P. Repetto, "Experimental power curve of small-size wind turbines in turbulent urban environment," *Appl. Energy*, vol. 154, pp. 112–121, Sep. 2015, doi: 10.1016/j.apenergy.2015.04.117.

[36] Q. Zhao and C. Cui, "Research on optimal gradient–climbing algorithm in wind power generation," *Appl. Mech. Mater.*, vols. 385–386, pp. 1100–1103, Aug. 2013, doi: 10.4028/www.scientific.net/amm.385-386.1100.

[37] C. Chatri, M. Ouassaid, M. Labbadi, and Y. Errami, "Integral-type terminal sliding mode control approach for wind energy conversion system with uncertainties," *Comput. Electr. Eng.*, vol. 99, Apr. 2022, Art. no. 107775, doi: 10.1016/j.compeleceng.2022.107775.

[38] V.-P. Vu, V.-T. Ngo, V.-D. Do, D.-N. Truong, T.-T. Huynh, and T. D. Do, "Robust MPPT observer-based control system for wind energy conversion system with uncertainties and disturbance," *IEEE Access*, vol. 9, pp. 96466–96477, 2021, doi: 10.1109/ACCESS.2021.3094819.

[39] A. Kashaganova, K. Suleimenov, S. Sagnaeva, and T. D. Do, "Maximum power tracking for wind energy conversion systems via a high-order optimal disturbance observer-based LQR without a wind speed sensor," *Eng. Sci. Technol., Int. J.*, vol. 45, Sep. 2023, Art. no. 101472, doi: 10.1016/j.jestch.2023.101472.

[40] B. Sarsembayev, N. Zhakiyev, A. Kushekkaliyev, K. Kayisli, and T. D. Do, "Output regulation-based optimal control system for maximum power extraction of a machine-side power converter in variable-speed WECS," *IEEE Access*, vol. 12, pp. 8422–8431, 2024, doi: 10.1109/ACCESS.2024.3352546.

[41] T. D. Do, "Disturbance observer-based fuzzy SMC of WECSs without wind speed measurement," *IEEE Access*, vol. 5, pp. 147–155, 2017, doi: 10.1109/ACCESS.2016.2633271.

[42] O. C. Castillo, V. R. Andrade, J. J. R. Rivas, and R. O. González, "Comparison of power coefficients in wind turbines considering the tip speed ratio and blade pitch angle," *Energies*, vol. 16, no. 6, p. 2774, Mar. 2023, doi: 10.3390/en16062774.

[43] A. V. Le and T. D. Do, "High-order observers-based LQ control scheme for wind speed and uncertainties estimation in WECSs," *Optim. Control Appl. Methods*, vol. 39, no. 5, pp. 1818–1832, Sep. 2018, doi: 10.1002/oca.2444.

[44] V. B. M. Krishna, V. Sandeep, S. S. Murthy, and K. Yadlapati, "Experimental investigation on performance comparison of self excited induction generator and permanent magnet synchronous generator for small scale renewable energy applications," *Renew. Energy*, vol. 195, pp. 431–441, Aug. 2022, doi: 10.1016/j.renene.2022.06.051.

[45] A. G. Abo-Khalil, A. M. Eltamaly, R. P. Praveen, A. S. Alghamdi, and I. Tlili, "A sensorless wind speed and rotor position control of PMSG in wind power generation systems," *Sustainability*, vol. 12, no. 20, p. 8481, Oct. 2020, doi: 10.3390/su12208481.

[46] A. B. Alhassan and T. D. Do, "Influence of higher-order disturbance estimation on maximum power extraction of wind energy conversion system using sliding mode control," in *Proc. 4th Int. Conf. Smart Grid Renew. Energy (SGRE)*, Jan. 2024, pp. 1–6, doi: 10.1109/sgre59715.2024.10428697.

[47] T. Roskilly and R. Mikalsen, *Marine Systems Identification, Modeling and Control*. Oxford, U.K.: Butterworth-Heinemann, 2015, doi: 10.1016/C2013-0-18786-7.

[48] J. A. Moreno and M. Osorio, "A Lyapunov approach to second-order sliding mode controllers and observers," in *Proc. 47th IEEE Conf. Decis. Control*, Cancun, Mexico, Jan. 2008, pp. 2856–2861, doi: 10.1109/CDC.2008.4739356.

[49] A. B. Alhassan, M. A. Shehu, B. B. Muhammad, S. Akbar, R. Chancharoen, and G. Phanomchoeng, "Sliding mode observer-based super-twisting controller for under-actuated bridge cranes subject to double-pendulum effect," *IEEE Access*, vol. 11, pp. 100695–100706, 2023, doi: 10.1109/ACCESS.2023.3315321.

[50] H. K. Khalil, *Nonlinear Systems*, 3rd ed., Upper Saddle River, NJ, USA: Prentice-Hall, 2002.
[51] T. D. Do and H. T. Nguyen, "A generalized observer for estimating fast–varying disturbances," *IEEE Access*, vol. 6, pp. 28054–28063, 2018, doi: 10.1109/ACCESS.2018.2833430.
[52] K. Suleimenov, B. Sarsembayev, B. D. H. Phuc, and T. D. Do, "Disturbance observer-based integral sliding mode control for wind energy conversion systems," *Wind Energy*, vol. 23, no. 4, pp. 1026–1047, Apr. 2020, doi: 10.1002/we.2471.

AHMAD BALA ALHASSAN (Member, IEEE) received the B.Eng. degree in electrical engineering from Bayero University, Kano, Nigeria, in 2011, the M.Eng. degree in mechatronics and automatic control from the University of Technology Malaysia (UTM), in 2016, and the Ph.D. degree in mechanical engineering from Xi'an Jiaotong University, China, in 2022. He was with the Department of Mechanical Engineering, Chulalongkorn University, Thailand, as a Postdoctoral Researcher, in 2023. He is currently a Postdoctoral Scholar with the Department of Robotics and Mechatronics, Nazarbayev University, Kazakhstan. He has authored or co-authored many research articles and international conference papers on dynamic analysis and control of crane systems, inverted pendulums, rehabilitation robots, elderly-assistant robots, power transmission line inspection robots, and wind energy conversion systems. His current research interests include modeling, simulation, and control of mechatronic systems. He has been a member of the IEEE Young Professionals, the IEEE Control Systems Society, and the IEEE Industrial Electronics Society. He was a Technical Session Chair at the IECON 2024 Conference, Chicago, USA. He has also served as a Reviewer for many refereed journals, including IEEE Access, *Journal of Mechanical Science and Technology*, and *Robotics and Autonomous Systems*.

MUHAMMAD AUWAL SHEHU received the B.Eng. degree in electrical engineering from Bayero University Kano (BUK), Nigeria, in 2012, and the M.Eng. degree in mechatronics and automatic control from the University of Technology Malaysia (UTM), in 2016. He is currently pursuing the Ph.D. degree in robotics engineering with Nazarbayev University, Kazakhstan. He has contributed several research articles to esteemed journals and conferences, establishing himself as a promising Researcher in his field. His primary research interests include the design of nonlinear control systems and state estimators for underactuated mechatronic systems.

VIJAYAKUMAR GALI (Senior Member, IEEE) received the master's degree from the Government College of Engineering, Kannur, India, in 2013, and the Ph.D. degree in power electronics from the Malaviya National Institute of Technology, Jaipur, India, in 2019. He has been a Senior Lecturer with the School of Physics, Engineering, and Computer Science, University of Hertfordshire, U.K., since June 2024. He has held notable positions, including a Postdoctoral Fellow with Nazarbayev University, Kazakhstan, from 2021 to 2024, where he led a project on dynamic energy management in smart grids. Previously, he was an Assistant Professor with Poornima University and JECRC Foundation, India. As a prolific author of research articles and conference papers, his contributions significantly impact sustainable energy systems and smart microgrids. His expertise continues to shape advancements in power system resilience and renewable energy technologies worldwide. His research interests include power electronics, renewable energy, smart grids, and digital twin models for power systems.

TON DUC DO (Senior Member, IEEE) received the B.S. and M.S. degrees from Hanoi University of Science and Technology, Hanoi, Vietnam, in 2007 and 2009, respectively, and the Ph.D. degree from Dongguk University, Seoul, South Korea, 2014, all in electrical engineering.

From 2008 to 2009, he was with the Division of Electrical Engineering, Thuy Loi University, Vietnam, as a Lecturer. He was a Postdoctoral Researcher with the Division of Electronics and Electrical Engineering, Dongguk University, in 2014. He was also a Senior Researcher with the Pioneer Research Center for Controlling Dementia by Converging Technology, Gyeongsang National University, South Korea, from May 2014 to August 2015. Since September 2015, he has been an Assistant Professor and promoted to an Associate Professor with the Department of Robotics and Mechatronics, Nazarbayev University, Kazakhstan. His research interests include control engineering, electric drives, renewable energy conversion systems, and nanorobots. He received the Best Research Award from Dongguk University, in 2014; the Most Cited Paper Award from Wind Energy, in 2020 and 2021; and the Outstanding Associate Editor Award of IEEE Access, in 2021, 2022, and 2023. He also received the Medal from the Minister of Science and Education for outstanding contribution to science in Kazakhstan, in 2024. He has been listed in the top 2% of scientists based on the citation on the single-year table, since 2019, and career-wide table, since 2021. He has been an Associate Editor of IEEE Access, from April 2017 to August 2024, and IEEE Robotics and Automation Letters, since August 2023. He has been promoted to be a Senior Editor of IEEE Access, since July 2024. He has been also a Guest Editor for special issues of several journals, such as *Mathematical Problems in Engineering*, *Electronics*, *Energies*, *Sensors*, *Fractal and Fractional*, and *International Journal of Advanced Robotic Systems*.